Summer 7-16-2018

Evaluating the Utility of Object-Based Image Analysis for Ecological Monitoring of Pinon-Juniper Mortality

Zachary C. Taraschi
The University of New Mexico

Zachary Taraschi

Candidate

Geography & Environmental Studies

Department

This thesis is approved, and it is acceptable in quality and form for publication:

Approved by the Thesis Committee:

Caitlin L. Lippitt, Chairperson

Christopher D. Lippitt

Marcy E. Litvak

EVALUATING THE UTILITY OF OBJECT-BASED IMAGE ANALYSIS FOR ECOLOGICAL MONITORING OF PIÑON-JUNIPER MORTALITY

By

ZACHARY TARASCHI

B.S. Geography, New Mexico State University
2015

THESIS

To Be Submitted in Partial Fulfillment of the
Requirements for the Degree of

Master of Science
Geography

The University of New Mexico
Albuquerque, New Mexico

July, 2018

Dedications

For my late Grandfather, Jim

To my parents, Tamalyn and James,
and my siblings Danielle, David and Katie

Acknowledgements

First, I would like to thank my advisor, Dr. Caitlin Lippitt, for her unyielding support, guidance, knowledge and encouragement through this process for whom without this would not be possible. Second, I would like to thank my two committee members, Dr. Chris Lippitt and Dr. Marcy Litvak, for their feedback and support.

The GEM Lab of UNM, specifically Su Zhang, Rowan Converse and Jesse Sprague for help during field collection. Dr. Chris Lippitt through the GEM Lab for data and the processing power to complete this thesis. The Litvak Lab of UNM for data and support when visiting the Deer Creek Plateau.

A world of gratitude to the UNM Department of Geography and Environmental studies faculty for all of the help and encouragement; Dr. Maria Lane, Dr. Chris Duvall, Dr. Yan Lin, Dr. Xi Gong, Dr. John Carr and Mindy Benson. GES Staff Texanna Martin and Sean O'Neill for all of the technological, emotional and administrative help they provided. And to Laura Gleasner of the Earth Data Analysis Center for her support with image data.

To all of my friends Hayley Hajic, Sagert Sheets, Aron Roberts, Jacob Wolff, Hanes Motsinger, Gladys Valentin, Anthony Meluso, Drake Miller, Renee Miller, Margo Ottesson, John Paustian, Ryan Blickem, Whitney Biel, Terry Casey, Shawn Casey, Rebecca Bellum and Gwen Walker. To my parents, Tamalyn Fraley and James White and to the entire Taraschi/White Family. Also, to the entire Lovato/Jojola family for their encouragement and support.

Finally, to my supportive and understanding significant other and partner in crime Alyssa Jojola, for whom without this would not have been a reality.

EVALUATING THE UTILITY OF OBJECT-BASED IMAGE ANALYSIS FOR ECOLOGICAL MONITORING OF PIÑON-JUNIPER MORTALITY

By

ZACHARY TARASCHI

B.S. Geography, New Mexico State University, 2015

M.S. in Geography, University of New Mexico, 2018

Abstract

Forested ecosystems in the American Southwest are experiencing change at an unprecedented rate, largely due to mortality events triggered by increased temperatures, drought, and insect infestations. Large-scale changes in the distributions of these ecosystems can potentially alter regional-scale carbon, water and energy dynamics. One biome in particular that has experienced increased mortality and altered forest composition over the past 30 years are Piñon-Juniper woodlands (*Pinus edulis, Juniperus* spp.) in the American Southwest. New fields of study, in particular, Remote Sensing, are applying and adapting traditional methods for ecological monitoring of these woodlands. Remote sensing offers the potential to synoptically classify and quantify specific tree species within mixed communities such as Piñon-Juniper (PJ) woodlands. This thesis tests the utility and reliability of an Object-Based Image Analysis (OBIA) classification applied to Very-High Resolution (VHR) imagery fused with historical National Agricultural Imagery Program (NAIP) imagery for detecting and quantifying piñon-pine mortality trends on a plateau of PJ woodland in Central New Mexico. Specifically, the research seeks to determine: (1) the accuracy of OBIA applied to VHR imagery for quantifying live PJ and dead piñon; and (2) the potential of NAIP data for creating an ecological timeline of forest mortality from 2005-2014. The OBIA process generated an overall classification accuracy of over 70%, whereas the time-series analysis using NAIP resulted in an overestimation of piñon mortality when compared to two sample-plots at the region.

Table of Contents

List of Figures

List of Tables

Chapter 1 Introduction

Forested ecosystems in the American Southwest are experiencing change at an unprecedented rate, largely due to mortality events triggered by increased temperatures, drought, and insect infestations (Allen et al. 2010). Higher temperatures and extended droughts over the last two decades provided longer time periods that are favorable for insect infestations of forest systems (Gaylord et al. 2013). Since the late 1890's, there have been six significant drought periods in the American Southwest; with the longest occurring from 1943 to 1957 and the most severe occurring in 2011-2013 over 80% of the contiguous United States (US), including the Southwest (Breshears et al. 2009; Williams et al. 2010; South Central Climate Science Center 2013; Ortiz, Breidenbach, and Kändler 2013). Die-off of piñon-pine (*Pinus edulis*), a critical component of piñon-juniper (PJ) woodlands (the fourth largest biome in the US), is a result of these periods of drought, rising temperatures, and pine beetle infestation (Williams et al. 2010; Gaylord et al. 2013). Quantifying the changes PJ woodlands experience in response to climate at a local scale may increase our understanding of the changes occurring across this biome at more of a regional scale.

Recent research into these woodlands at a regional scale used remotely sensed imagery to classify and quantify woodland distributions and mortality (Clifford, Cobb, and Buenemann 2011); while other research focused on more localized areas to compare with in-field ecological data (Eitel et al. 2011; Krofcheck et al. 2014; Brewer et al. 2017). Remote sensing offers several advantages over traditional ecological monitoring methods: it provides a synoptic view, is generally unobtrusive to the environment, and can provide a temporal catalogue of change over time. With these advantages, the ability

to accurately classify and quantify specific tree species within mixed communities such as PJ woodlands is challenging (Clifford, Cobb, and Buenemann 2011). Beyond the communities themselves, differentiating between piñon and juniper is challenging using remotely sensed imagery, as the two species have similar spectral profiles, and are distributed in mixed patches (Brewer et al. 2017). It's the mixed nature of this community type that limits the classification of these woodlands; even with a fine spatial resolution, mixed PJ patches are what can be derived (Eitel et al. 2011; Brewer et al. 2017).

Accurately classifying these mixed patches requires imagery at finer scales defined as Very High Resolution (VHR) (Clifford, Cobb, and Buenemann 2011; Colomina and Molina 2014). VHR, being a more recent paradigm in the field of remote sensing, currently allows for only one viable classification methodology: Object-Based Image Analysis (OBIA) (Blaschke 2010; Colomina and Molina 2014). OBIA is a multi-step classification method where high-resolution images are segmented into object specific features based on characteristics such as location, proximity, and spectral homogeneity (Strahler, Woodcock, and Smith 1986; Blaschke et al. 2014). OBIA differs from traditional classification methods by describing scene phenomena as discrete objects (h-resolution), rather than individual spectral values contained within single pixels (Strahler, Woodcock, and Smith 1986; Blaschke 2010).

Using the high-resolution boundaries of PJ provided by the OBIA classification allows for identification of these patches in data with coarser spatial resolution but with a higher temporal resolution (Maxwell 2011). By applying a Normalized Difference Vegetation Index (NDVI) (Rouse et al. 1973) transformation constrained to the boundaries set by the OBIA classification, an evaluation of PJ health can be made over

many years (Gandhi et al. 2015). This evaluation can then be used to draw upon spatial distributions of mortality over many years of data with respect climatological events (Stoyan and Penttinen 2000).

It's through these lenses that this thesis seeks to test the utility and reliability of using high spatial resolution remotely sensed imagery for detecting piñon mortality in Central New Mexico. An OBIA-based image classification of VHR imagery was used in conjunction with historical National Agricultural Imagery Program (NAIP) imagery to track mortality related to a recent drought period. Specifically, the research determines: (1) the accuracy of OBIA applied to VHR imagery for quantifying live PJ and dead piñon; and (2) the potential of NAIP data for creating an ecological timeline of forest mortality from 2005-2014.

Chapter 2 Background

2.1 Piñon-Juniper Woodlands

PJ Woodlands are one of the most commonly found vegetation types in the American Southwest, are and are distributed from northern Utah to south-central New Mexico at elevations ranging from 1,370 to 2,290 meters above mean sea level (National Park Service 2017). PJ woodlands are heavily studied because of their widespread distribution throughout the Southwest, cultural significance, utility as a food and wood resource, and patterns of mortality in response to periods of drought (Evans and USDA Forest Serivce 1988; Allen et al. 2010). Current mortality in PJ woodlands throughout the Southwest is related to a combination of increased temperatures, insect infestations, and recent drought

events in the early 2000's (Shaw, Steed, and DeBlander 2005; Mueller et al. 2005), and more recently from 2009-2011 (Williams et al. 2012; Meddens et al. 2015).

Williams et al. 2010 forecasted that previous weather and drought conditions can be used as a proxy to model future trends in response to predicted climate scenarios. Vegetation communities, like PJ woodlands can be used as a proxy to better understand the severity of droughts at a regional/local level (Allen et al. 2010). On a more localized level, the two most recent drought events in the Middle Rio Grande region of New Mexico triggered mortality (average rate of 54% for piñon during the first event) and stressed piñons to a state that allowed beetle infestation during the second event (Gaylord et al. 2013; Meddens et al. 2015). Current predictions suggest that frequency and duration of these climate events are accelerating (IPCC 2014), prompting techniques and models that aid in a better understanding of potential future changes in climate and vegetation.

2.2 Remote Sensing of Vegetation

Beyond visualization, remote sensing analysis is used to record and transmit information beyond the capacity of the human eye and allows for a temporal record of change (Jensen 2005). The ability to sense wavelengths beyond the visible portion of the electromagnetic spectrum (EMS) offers a distinct advantage in the detection and classification of certain vegetation types over traditional vegetation mapping methods. Healthy vegetation reflects very little in the visible portion of the EMS, but has a peak in the green region due to chlorophyll content, (Roberts, Smith, and Adams 1993). As leaves become physiologically stressed, less able to photosynthesize, and chlorophyll content reduces, reflectance increases in the blue and red regions and decreases in the green region (Jensen

2005). Even with this dynamic reflectance in the visible spectrum, vegetation has peak reflectance in the near-infrared (NIR) indicating when vegetation are healthy, diseased, stressed, or entering senescence (Knipling 1970). Being the main tool for the remote sensing of vegetation, the ability to record and quantify the NIR portion of the EMS also constitutes the building blocks for vegetation indices (Jensen 2005).

2.2.1 Normalized Difference Vegetation Index (NDVI)

NDVI is one of the most widely employed spectral vegetation indices used by remote sensing scientists. Vegetation indices are dimensionless, radiometric measures. NDVI indicates the abundance and activity of green vegetation (Jensen 2005), and only requires two spectral bands: red and NIR (Rouse et al. 1973). Healthy vegetation absorbs most visible light for photosynthesis and reflects NIR wavelengths due to the turbid, water filled cells of its spongy mesophyll (Knipling 1970). The difference between these two spectral regions indicates photosynthetic activity or stress status of vegetation in imagery. NDVI was first used by Rouse et al. (1973) and outputs pixel values ranging from -1 to 1, with higher values implying a higher concentration of photosynthetically active vegetation.

NDVI is given below (eq. 1):

$$\text{NDVI} = \frac{NIR-RED}{NIR+RED} \qquad \text{eq. 1}$$

NDVI values can change between species based on physiological stress, resulting from the percent of NIR energy reflected by the specimen (Knipling 1970). Changes in NDVI can be used to create threshold values to better quantify vegetation health (Gandhi

et al. 2015). NDVI thresholding was successfully used for studying vegetation change (Gandhi et al. 2015) and to model vegetation mortality (Sonwalkar, Fang, and Sun 2010). NDVI is one of the most widely used applications of imagery gathered by the National Agriculture Imagery Program (NAIP).

The primary directive of NAIP is to acquire aerial imagery during the agricultural growing seasons and make orthophotos available to governmental agencies and the public within a year of acquisition within the continental US (USDA Farm Service Agency 2006). This data is acquired at a one meter spatial resolution in four spectral bands: near-infrared, red, green, and blue, and is output in digital ortho quarter quad (DOQQ) tiles (USDA Farm Service Agency 2006). Currently acquired on a three-year cycle, NAIP has been leveraged for a wide variety of applications. Davies et al. (2010) used NAIP data to relate juniper cover to environmental variables and (Moskal, Styers, and Halabisky 2011) for monitoring urban tree coverage. Hayes, Miller, and Murphy (2014) reported high accuracy land cover classifications using NAIP data; and Hulet et al. (2014) found success using NAIP data for mapping distribution and biomass of piñon-juniper woodlands.

2.4 Object-Based Image Analysis

Spatial resolutions ranging from sub-centimeter to one-meter are considered to be VHR. In most cases, VHR imagery analysis employs the H-resolution scene model, where objects are represented by many pixels (Strahler, Woodcock, and Smith 1986; Lippitt 2015). This differs from the traditional paradigm of remote sensing, which traditionally relied on L-resolution scene models where one pixel may represent a mixture of discrete

objects (Strahler, Woodcock, and Smith 1986; Lippitt 2015). OBIA is a non-traditional paradigm of remote sensing, and the only current commercially available processing technique that can be leveraged to interpret and classify an H-resolution scene model (Lippitt 2015).

OBIA uses groups of pixels, or segments, to form objects to classify a scene. In contrast, traditional pixel-based classifiers use spectral values of individual pixels (Ryherd and Woodcock 1996). The OBIA process begins by creating machine-defined segments based on the spectral homogeneity of pixels. From the segmented image, a user then creates a classification model to define how segments will be classified either by defining rules through a decision tree or by choosing example segments for objects. The OBIA workflow is an iterative process of defining classes from objects to yield a final classification of the image (Blaschke et al. 2014).

While VHR imagery is typically limited to visible and near-infrared bands, the inclusion of textural and spatial information in addition to spectral information lets OBIA classify this imagery more efficiently than traditional pixel-based approaches, which rely solely on spectral data (Laliberte et al. 2007). Several studies (Kamal, Phinn, and Johansen 2015; Lehmann et al. 2015; Knoth et al. 2013) report high classification accuracies using OBIA applied to VHR imagery.

Utilizing the resolutions of VHR imagery, OBIA can be employed to monitor and classify specific vegetation types. Specifically, Laliberte et al. (2011) recorded high accuracies when compared to commercially available satellite options for rangeland vegetation in southern New Mexico. Knoth et al. (2013) recorded accuracies over 91% for specific species when measuring and quantifying vegetation health in response to

restoration efforts following deforestation in northwest Germany. Finally, Lehmann et al. (2015) used OBIA and VHR with great success to classify beetle infested trees in western Germany.

Using OBIA to classify at this resolution creates discrete boundaries of the vegetation types being studied. These boundaries can subsequently be applied to datasets at a coarser resolution than the VHR imagery they were derived from (Maxwell 2011). NAIP has a coarser spatial resolution but a greater temporal frequency than VHR imagery, and thus, can be used to create a timeline of vegetation health and mortality (Davies et al. 2010).

2.6 Assessing Patterns of Mortality

Recent trends for detecting change in woodland composition and mortality use methods that convert individual stand or patch level data collected from the field to vector polygons (Stoyan and Penttinen 2000; Liu et al. 2007). Patch level NDVI data allows for generation of thresholds to distinguish live and dead vegetation (Gandhi et al. 2015). NDVI thresholds are used to describe structural changes in woodland composition related to increasing or decreasing vegetation health (Gandhi et al. 2015). By using NDVI thresholds to quantify a ratio of live to dead, a patch level assessment of mortality can be derived (Liu et al. 2007). When applied to datasets from prior years, changes in vegetation health can be modeled, providing a temporal record of vegetation change (Gandhi et al. 2015).

These patch level data can be further evaluated with a variety of spatial statistical tests (Stoyan and Penttinen 2000). Specifically, the Moran’s I test, a measurement of

spatial autocorrelation in relation to neighbors (Moran 1950), is used to describe woodland mortality on a neighborhood basis (Stoyan and Penttinen 2000; Liu et al. 2007). By way of comparing decreasing values in NDVI on a neighborhood basis, inferences about mortality beyond drought and temperature (pine beetle infestation, water uptake, etc.) in woodland systems can be made (Stoyan and Penttinen 2000; Meddens et al. 2015; Morillas et al. 2017).

Chapter 3 Methodology

An OBIA classification was applied to VHR color-infrared (CIR) imagery acquired in 2014 over the Deer Creek Plateau (DCP) to classify dominant vegetation community-types into five classes: live piñon-juniper, dead piñon-juniper, shrub, herbaceous, and bare ground. From this classification, a vector layer of live and dead piñon-juniper segments was extracted. A multi-step python toolbox was created to apply the vector layer of live PJ and dead piñon segments to the 2005, 2009, 2011, and 2014 NAIP imagery. NDVI thresholding of mean segment NDVI values from NAIP was used to generate an ecological timeline of piñon mortality for the plateau.

3.1 Study Area

The study area for this research is located on a plateau approximately 8 km south of the town of Mountainair, New Mexico (Figure 1). The Litvak lab is running two eddy covariance towers here, one of which is an Ameriflux core site (34º 26′ 55” N, 106º 14’ 44” W). The other flux tower is 5 km away, installed through DOE funded research to

examine the consequences of piñon mortality on ecosystem scale fluxes (Krofcheck et al. 2014; Morillas et al. 2017). The region is dominated by piñon-juniper woodlands and ranges in elevation from 2,000 to 2,200 meters. The study region has a mean annual precipitation of 37.2 cm and a mean temperature of 67.6 °F (1984-2014) (PRISM Climate Group).

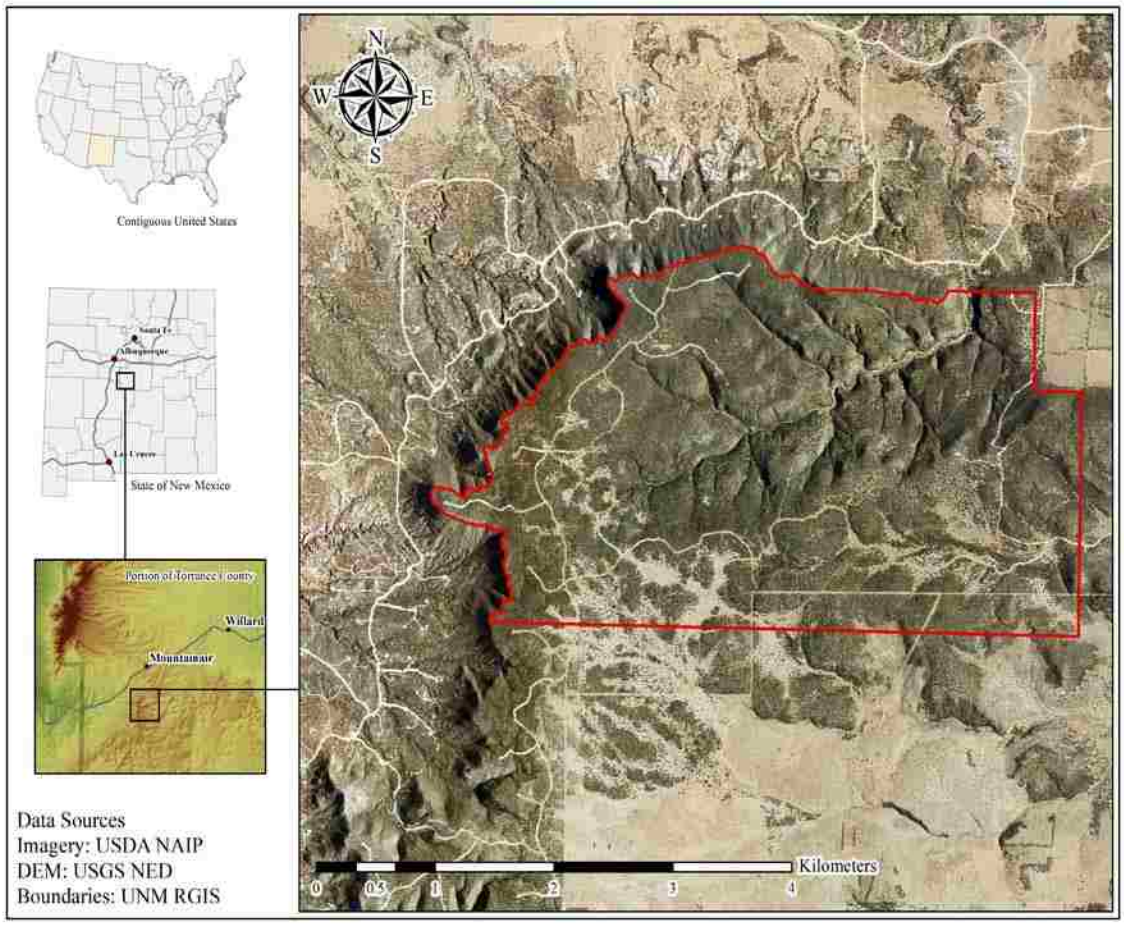

Figure 1. Map showing the Study Area (outlined in red) and DCP in reference to New Mexico and the United States.

3.2 Data

3.2.1 Image Data

The VHR imagery used in this study was acquired on September 2, 2014 using a GT500 ultralight aircraft (courtesy of the University of New Mexico Litvak & GIScience for Environmental Management (GEM) Labs). Two Canon 5D Mark II cameras were used to acquire the imagery; one camera recorded reflectance in red, green, and blue wavelengths, while the other camera recorded blue green, and NIR (800-900 nm) wavelengths. Together, these two cameras were used to acquire imagery for the entire Deer Creek Plateau at a nominal GSD of 7 cm. Four-band (B, G, R, NIR) NAIP data (1 m spatial resolution) for 2009, 2011, and 2014 were acquired from the Earth Data Analysis Center (EDAC) at The University of New Mexico (UNM).

3.2.2 Calibration and Validation Data

Classification calibration and validation data used in this study comes from multiple sources. Field-based reference data of dominant vegetation species were geo-located using a Trimble R10 RTK unit and a Garmin eTrex 20 hand-held receiver. These field-based reference points were used to select appropriate segments of live PJ and dead piñon within the imagery rather than using these points in a raw fashion; thereby reducing effects of spatial error. Image-based reference data were collected for herbaceous, bare ground and vegetation shade classes; these shade classes were included but are only applicable for the calibration data. Following classification, shade classes were merged with non-shade classes. A list of classes and the number of calibration and validation

points are shown in Table 1. A map showing the distribution of calibration and validation points in shown in Figure 2.

Table 1. Number of pixels per class selected for calibration/validation.

Class Name	Number of Calibration pixels	Number of Validation pixels
Live PJ	50	70
Dead Piñon	50	50
Herbaceous	50	70
Shrub	15	15
Bare Ground	35	55
Shaded Live PJ	20	N/A
Shaded Herbaceous	20	N/A
Shaded Bare Ground	20	N/A
Total	260	260

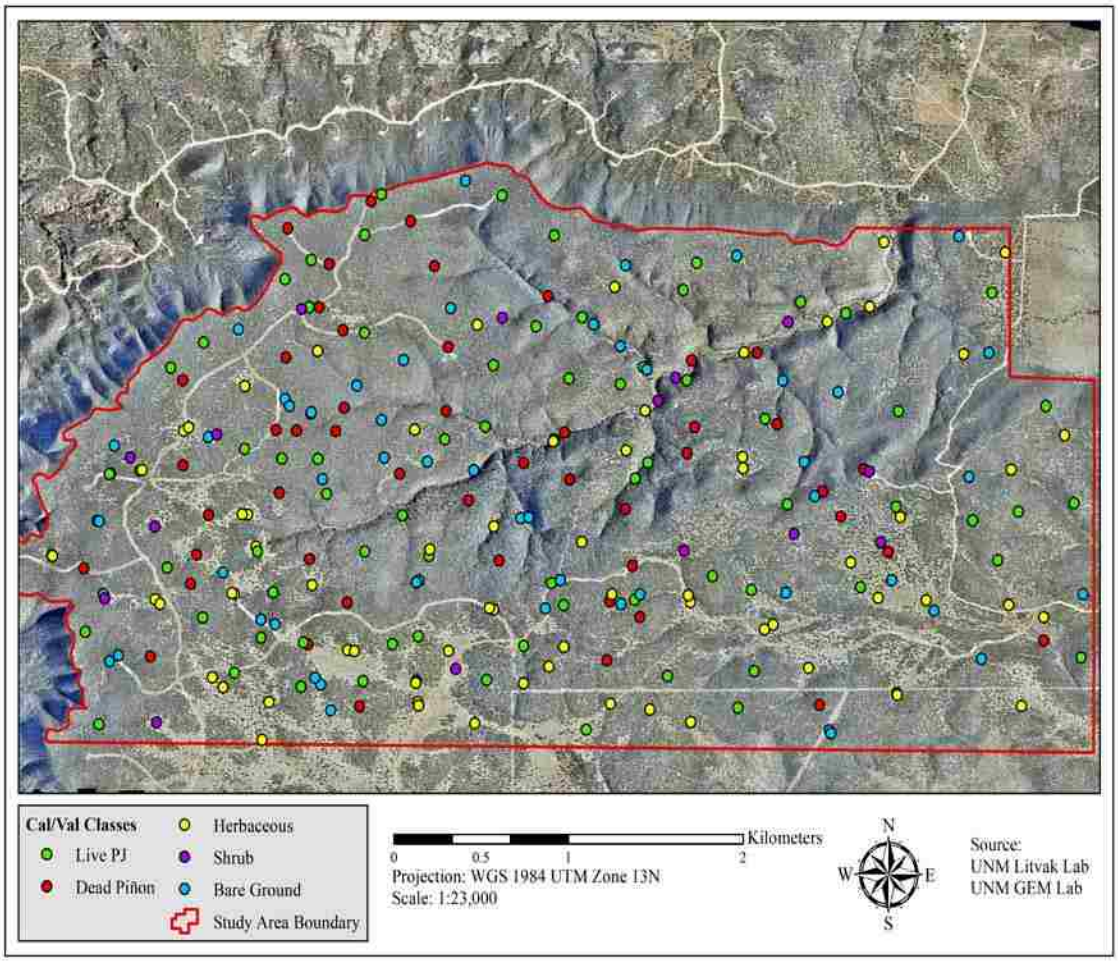

Figure 2. Map showing the distribution of calibration and validation data.

3.2.3 Climate Data

Climate data provided by the Litvak Lab at The University of New Mexico was used for the years 2008-2014. This data included mean daily precipitation and the mean daily temperatures for the study area as reported by the two flux towers at the plateau. This climate data was used for comparison with OBIA/NDVI based estimates of species decline and mortality with regards to changes in precipitation and temperature prior to, during, and following the 2009-2013 drought period.

3.3 Preprocessing

3.3.1 VHR Imagery

Several steps were required to process raw imagery into a format that could be used as an input for OBIA. Following image acquisition, images were converted from a raw to .jpg format by the GEM lab. In order to geometrically correct, reconstruct and mosaic imagery of the DCP from the 4,242 individual images, a structure-from-motion–multi-view stereo (SFM-MVS) process was used. To aid in the process of scene reconstruction, 16 GPS/GNSS points collected using a Trimble R10 RTK unit were introduced as control to the NIR,G,B pointcloud. These points were collected at the same time as the cal/val data. Following acquisition, these points had a post-differential correction applied (OPUS National Geodetic Survey), and were output with a combined root mean square error (RMSE) of less than 16 mm.

A pointcloud for the R,G,B images was then generated and aligned to the resultant NIR,G,B pointcloud. The NIR,G,B pointcloud was then used to create a digital surface model (DSM) at a spatial resolution of 27.8 cm. An NIR,G,B ortho-mosaic at a

spatial resolution of 7 cm with an overall RMSE of 16 cm (measured using independent ground control points) was generated using the DSM for terrain correction. The process was then repeated for the R,G,B pointcloud aligned to the NIR,G,B pointcloud. Finally, a 4-band orthophoto of NIR,R,G,B using a layer stack function was generated. Following the layer stack function, a forward principal component analysis (PCA) rotation was performed producing four PCA bands. An inverse PCA was performed using the first three PCA bands in order to transform the PCA bands back to the original imagery. The goal of the PCA was to reduce the effects of bidirectional reflectance distribution formula (BDRF) on the imagery. The final four-band VHR imagery is show in Figure 3**.**

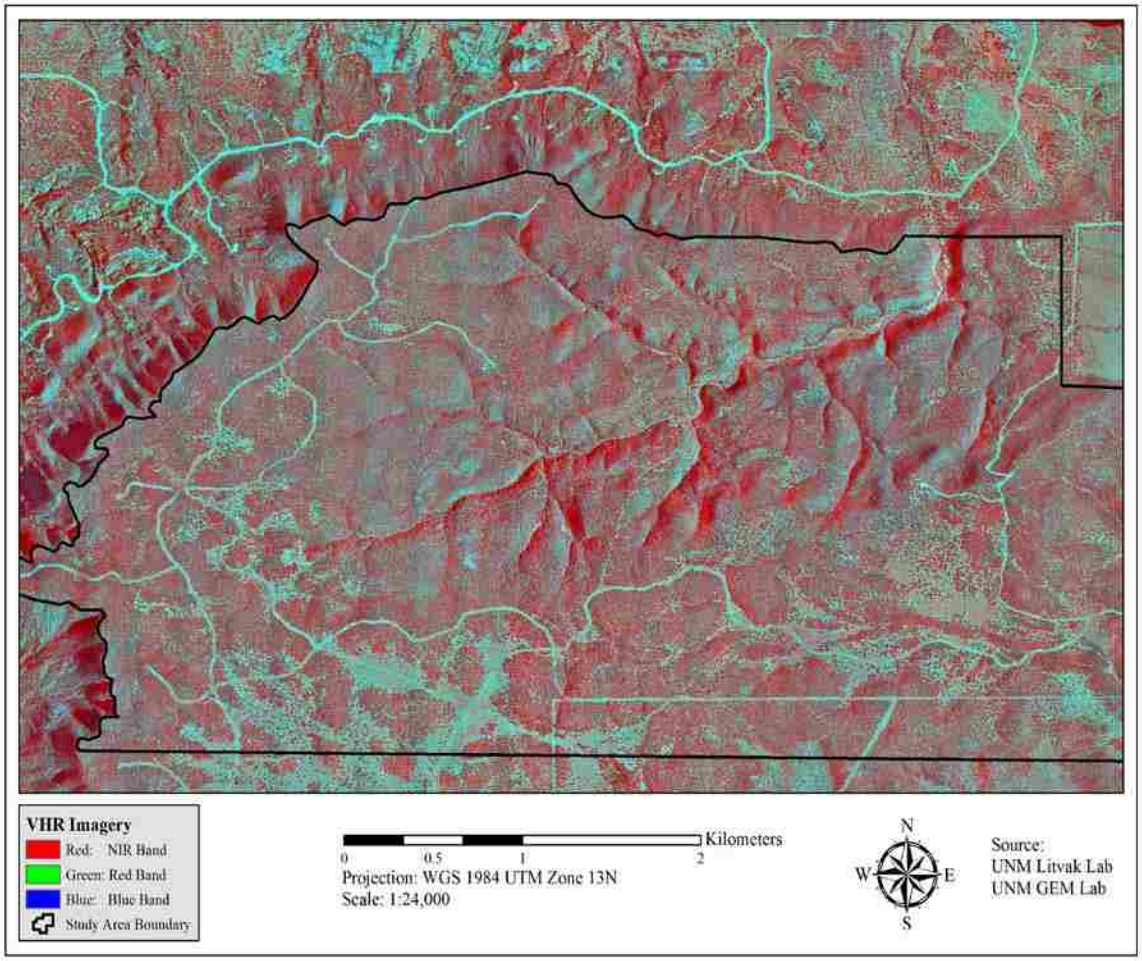

Figure 3. Color-Infrared orthophoto generated from VHR imagery.

3.3.2 NAIP Data

Geometric corrections were applied to the 2014 NAIP dataset using a second order polynomial transformation. This transformation was done using control points to align the dataset to the VHR imagery at an RMSE of 10 cm (measured using 10 check points). NAIP datasets for the years of 2005, 2009 and 2011 were referenced to the corrected 2014 dataset using a second order polynomial transformation at an RMSE of 50 cm.

3.4 OBIA Workflow

The 4-Band DCP orthomosaic was imported into Environment for Visualizing Images (ENVI)'s Feature Extraction (FX) module (Harris Geospatial 2008) for OBIA. Users have the option of using Rule or Example-based feature extraction methods, as shown in the workflow in Figure 4. The Example-based (Supervised) feature extraction method was selected for this study.

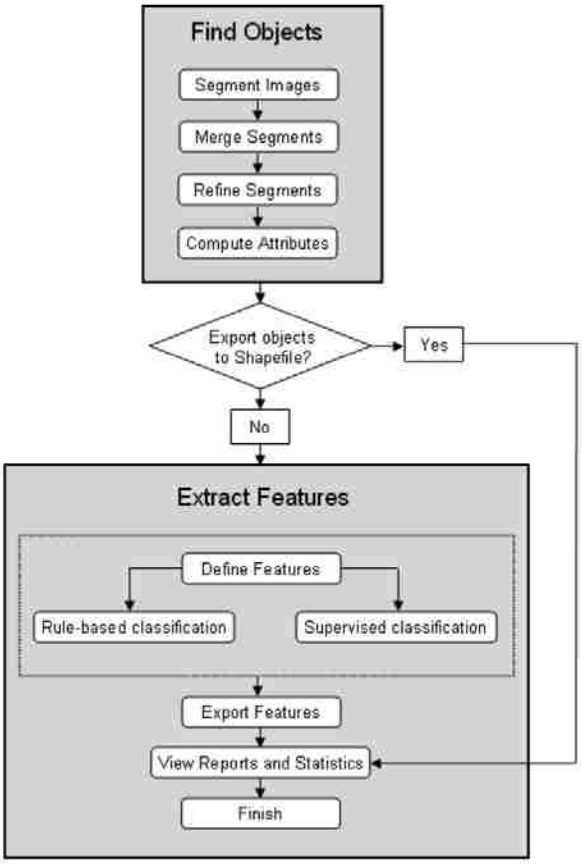

Figure 4. OBIA Workflow for ENVI Feature Extraction Module (Harris Geospatial 2008).

Roads were manually classified and masked out to reduce the effects of human-made changes to the environment prior to input into FX. An additional mask was created to remove areas affected by image blur. The mask was generated by exploring the imagery to identify areas of low-texture and manually classify these areas to prevent under-segmentation. These areas occur towards the center, but also in riparian areas, and in the south-east corner of the imagery. These areas are the byproducts of cameras losing focus during image acquisition.

The masked subset was input into FX for the first step in the OBIA process, image segmentation. Scale level, merge level, and texture kernel size were tested based

on analyzing specific areas of the study area, and by running example classifications. A Scale level (using the edge option) of 35% was ideal for deriving sharp boundaries between differing classes while maintaining computational efficiency. A full lambda schedule algorithm was used for the Merge level at a factor of 85% to merge together larger textured areas such as trees. The 85% merge factor provided the most complete segments between the woodland classes while preserving the boundaries between the other classes. Finally, a texture kernel size of 5 was implemented based on the size of pixels in comparison to the size of objects.

Following segmentation, “example” segments for each of the eight classes were selected using the calibration data as reference. Mean spectral profiles were generated for calibration and validation data to evaluate separability between classes (Figure 5).

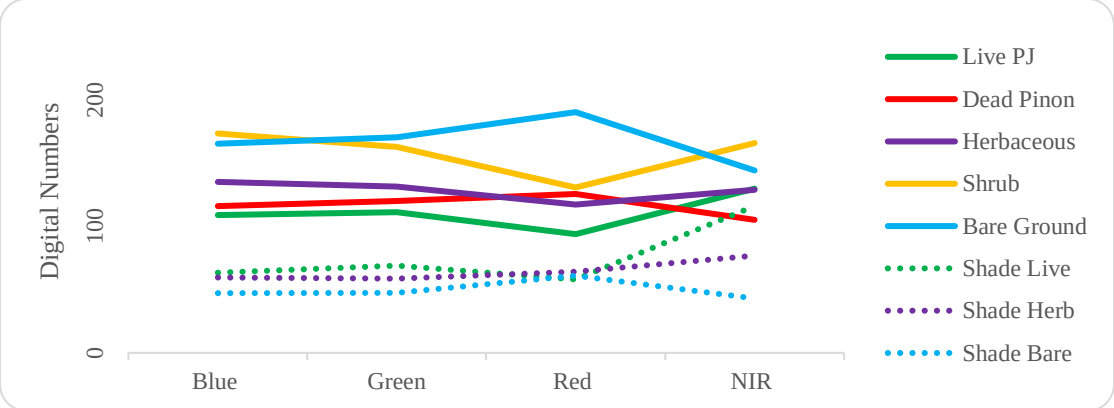

Figure 5. Mean spectral profiles of training segments used during image classification.

After selection of training data, a support vector machine (SVM) classifier was implemented. The SVM has been found to provide accurate results for complex data sets with little separability between classes (Harris Geospatial 2008). Along with the classification algorithm, input features for the classification were selected (Table 2). The

spectral attributes relate to the statistics of individual pixel values within each segment for each band of the VHR imagery. The texture attributes used are similar to the spectral attributes but relate to the statistics of the groupings of pixels within each example segment. The spatial attributes are geometric measurements of each example segment. These attributes were selected based on the complex nature of PJ canopies and were found to add the greatest amount of distinction between each class located in the study area based on trial and error. Further spatial attributes such as length, direction, etc. were available, but did not improve classification.

Table 2. Description of Classification Attributes used in OBIA (Harris Geospatial 2008).

Attribute	Description
Spectral	
Mean	Mean value of pixels for each band
Maximum	Maximum value of pixels for each band
Minimum	Minimum value of pixels for each band
Standard Deviation	Standard deviation of pixels for each band
Texture	
Range	Average data range of pixels comprising the region inside the kernel
Mean	Average value of pixels comprising the region inside the kernel
Variance	Average variance of pixels comprising the region inside the kernel
Entropy	Average entropy value of pixels comprising the region inside the kernel
Spatial	
Area	Total area of the polygon, minus the area of the holes.
Compactness	A shape measure that indicates the compactness of the polygon.
Convexity	A measure of the convexity of the polygon.
Solidity	A shape measure that compares the area of the polygon to the area of a convex hull surrounding the polygon.
Roundness	A shape measure that compares the area of the polygon to the square of the maximum diameter of the polygon.
Form Factor	A shape measure that compares the area of the polygon to the square of the total perimeter.
Elongation	A shape measure that indicates the ratio of the major axis of the polygon to the minor axis of the polygon.
Rectangular Fit	A shape measure that indicates how well the shape is described by a rectangle.
Number of Holes	The number of holes in the polygon.
Hole Area/Solid Area	The ratio of the total area of the polygon to the area of the outer contour of the polygon

3.5 Accuracy Assessment

Using the validation points, a confusion matrix was generated to assess the overall accuracy, user's/producer's accuracy, as well as a kappa coefficient of each classification. Overall accuracy is a measure of the number of validation pixels classified correctly divided by the total number of validation pixels; user's accuracy is the degree of commission (error of inclusion), and producer's accuracy is the degree of omission (error of exclusion) (Jensen 2005). Kappa coefficient within the matrix is a degree of agreement similar to overall accuracy, but differs by accounting for the probability of correct classification by chance based on training samples (Jensen 2005).

3.6 NDVI Thresholding

The one-meter resolution of the NAIP imagery makes it difficult to identify individual patches of piñon-juniper. To aid in the discrimination of live and dead patches, NDVI images were generated for each NAIP dataset using a multi-step python toolbox. The purpose of the toolbox is to subset rasters to a region, perform NDVI, extract mean values of NDVI at specific segments across multiple image datasets, and create a binary decision tree to label segments as live or dead based on these mean values. The "steps" for the python toolbox are individual modules, each module produces specific outputs.

The first module, hereafter referred to as Module 1, subsets the input rasters by a vector boundary, or "study area", and then performs an NDVI operation on each input raster layer. The process steps for Module 1 are shown in Figure 6. For this project, the input rasters included the NAIP data for 2005, 2009, 2011 and 2014, and the input vector

boundary was the study area for this project. From Module 1, NDVI rasters were output for each input year.

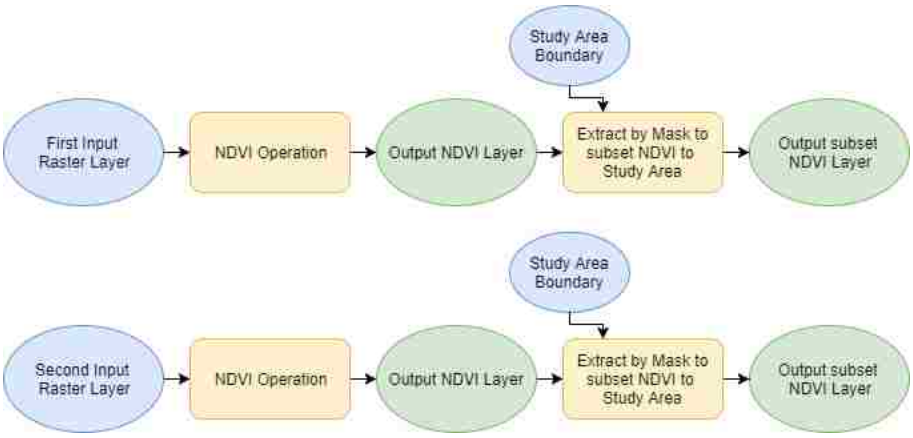

Figure 6. Workflow for Module 1.

The second step, Module 2, intersects the outputs from Module 1 with a vector boundary layer delineating live and dead segments. The input vector boundary was derived from the OBIA classification by taking the classification output, converting it to a vector format, selecting only live and dead PJ patches, and removing any artifacts from the layer.

Module 2 (Figure 7) was developed to convert NDVI pixels to point-vector values, and then perform a spatial join with the input polygon layer to generate NDVI values for live and dead PJ patches. After the spatial join is performed, cell values are then averaged within each patch, creating a vector layer of composite NDVI values. The second step in Module 2 uses the composite NDVI values for the first input year (2014) to define live and dead NDVI values for the other image dates.

Module 2 performs this process by creating a decision tree as shown in Figure 8. Module 2 uses this decision tree to make a binary decision creating class values of live

and dead for the years of data prior to the original input year, whereby positive NDVI is live and negative NDVI is dead. The OBIA outputs of live PJ and dead piñon were used to determine live and dead segments within the NAIP imagery. Using these locations, it would only select dead segments to determine if they were live for each prior year of data. For this project, Module 2 was used to output both a vector layer highlighting live and dead and a raster layer of composite NDVI values for individual PJ patches for the 2014 NAIP dataset, the same products were also output for the years of 2011, 2009 and 2005.

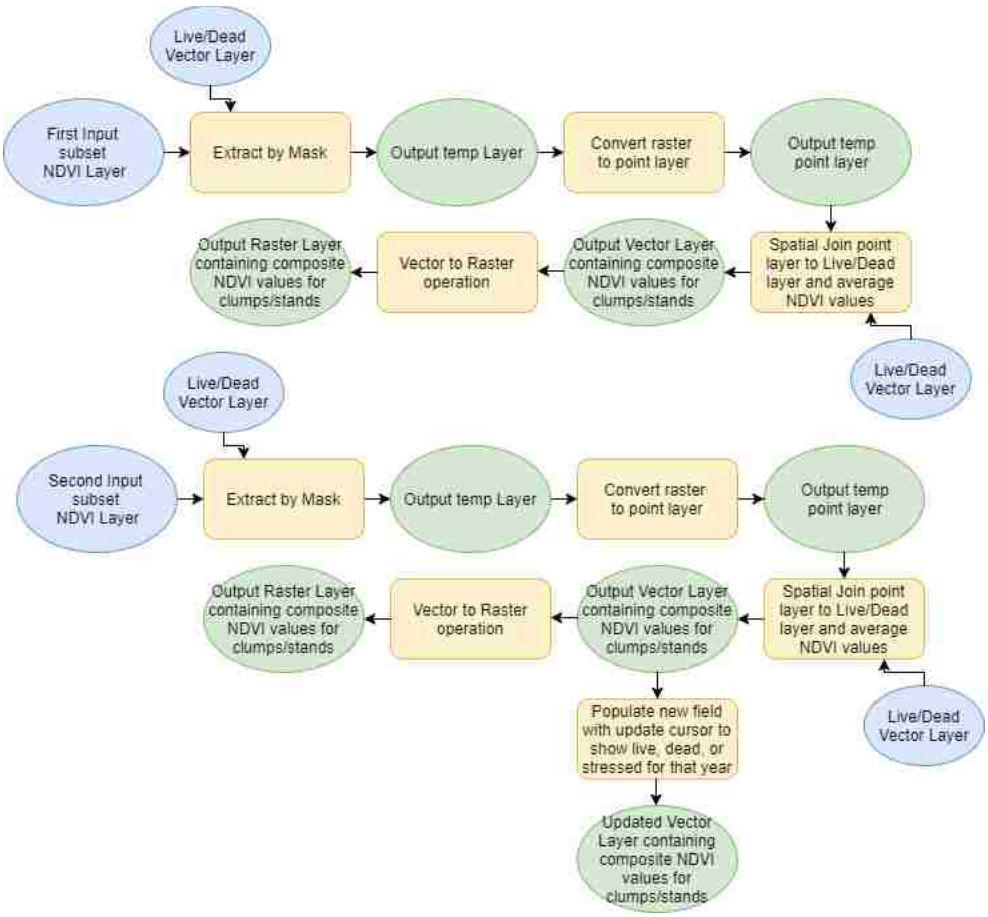

Figure 7. Workflow for Module 2.

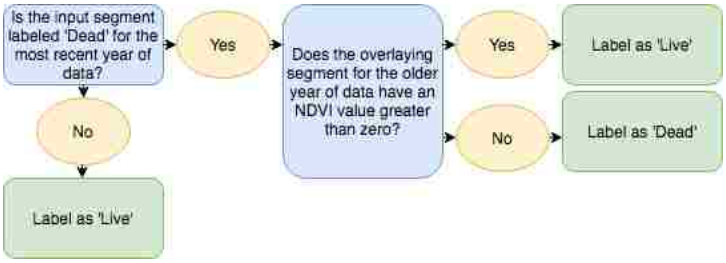

Figure 8. Decision Tree Workflow for labeling of Live/Dead PJ patches.

3.7 Piñon-Juniper Mortality and Change

To visualize a timeline of mortality across the plateau, the third step of the python toolbox was created, referred to as Module 3 (Figure 9). Following NDVI thresholding, a mask is applied to the vector layers output from Module 2 to display only 'new' dead PJ patches for each year. The module then generates a layer that combines all of the new dead patches for each image year. Image differencing (where the older NDVI dataset is subtracted from the more recent NDVI dataset) is then used to visualize and highlight NDVI changes between the study years. The final step of Module 3 computes a local Moran's I for each year of 'new' dead patches, to visualize neighborhoods of mortality for each year across the study area by testing for spatial autocorrelation.

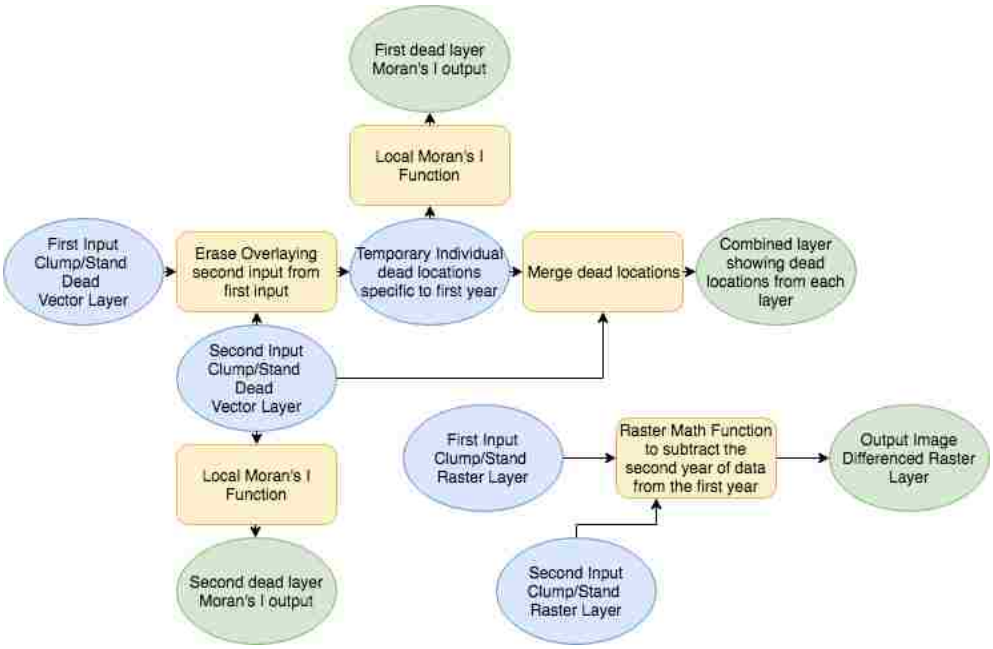

Figure 9. Workflow for Module 3.

Using Module 3, a single layer denoting dead patches of piñon specific to each year of NAIP data was output. Image differenced NDVI raster layers between 2005 and 2009, 2009 and 2011, 2011 and 2014, and throughout the study period (2005 to 2014) were also output**.** Finally, a local Moran's I for the new patches of dead piñon within each dataset was output.

In order to quantify change over time, these outputs from Module 3 were used to calculate the percentage of conversion from live to dead PJ for each year of the study period. Finally, a comparison of mortality and changes in vegetation distribution to daily readings of precipitation and mean temperature as collected by the Litvak Lab for the Deer Creek Plateau was performed.

Chapter 4 Results

Results are organized in three sections: 1) OBIA-based classification accuracy and 2014 vegetation distribution at the DCP, 2) an evaluation of mortality based on NDVI Thresholding, and 3) piñon mortality and change with respect to climate.

4.1 OBIA Classification Results

The outputs from OBIA included segmented and classified images. These were used to generate an accuracy assessment and classified maps. The classified maps were created for both the entire study area as well as over long-term research plots.

4.1.1 Accuracy Assessment

Results from the accuracy assessment are shown in confusion matrices (Table 3). Overall classification accuracy was 71.92%, and Kappa was 0.63. Producer's accuracy ranged from 91.43% (live PJ) to 26.67% (shrub) while user's accuracy ranged from 87.15% (dead piñon) to 57.14% (shrub). The classes with the highest accuracies were both live PJ and dead piñon. In some areas, live PJ was confused with both herbaceous and bare ground, and dead piñon was confused with herbaceous, bare ground and even live PJ at times.

Herbaceous and bare ground were difficult to distinguish, where based on omission error, 32.72% of the bare ground class was classified as herbaceous, and 14.28% of the herbaceous class was classified as bare ground. Herbaceous was also misclassified as live PJ (14.28%) and misclassification within the shrub class occurred most often with the live PJ class (33.33%).

Table 3. Confusion Matrix generated from the Validation Data

Class	Live PJ	Dead Piñon	Herbaceous	Shrub	Bare Ground	Total	User's Acc	Commission Error
Live PJ	64	3	10	5	1	83	77.12	22.88
Dead Piñon	0	42	4	2	1	49	85.71	14.29
Herbaceous	5	2	45	2	18	72	62.50	37.50
Shrub	0	0	1	4	2	7	57.14	52.86
Bare Ground	1	3	10	2	33	52	67.31	32.69
Total	70	50	70	15	55	260		
Producer's Acc	91.43	84	64.29	26.67	63.64			
Omission Error	8.57	16	35.71	73.33	36.36			
Overall Accuracy	= 71.92%		Kappa Coefficient	= 0.63				

4.1.2 Evaluation of OBIA Classified Maps

The vegetation map generated from OBIA classification is shown in Figure 10. Two well-known areas were selected for evaluating classification results: 1) the girdled site (PJG) in the eastern portion of the DCP, and 2) the control site (PJC) located in the south-central portion of the DCP (Figure 11).

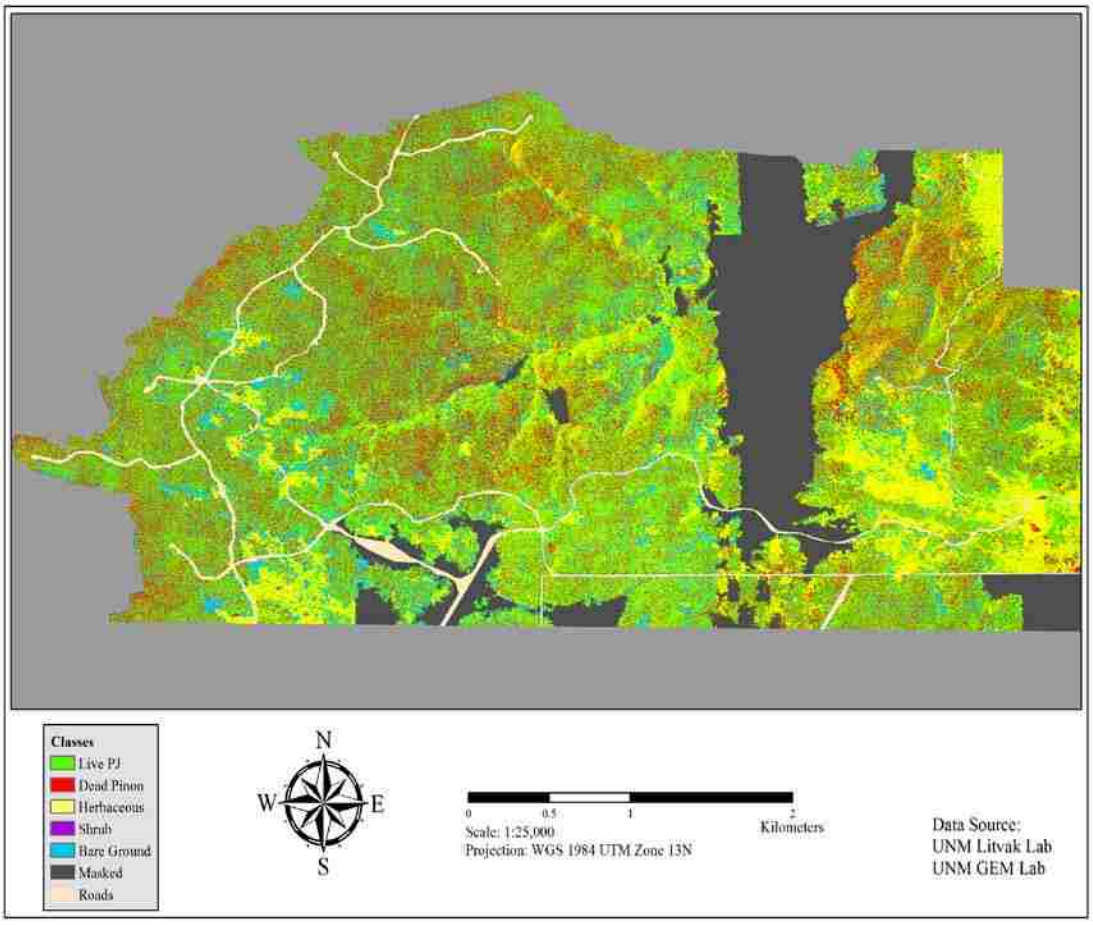

Figure 10. Map of the OBIA-based image vegetation classification for the Deer Creek Plateau.

Visually, the distribution of classes across the study area is similar to that of the input imagery where vegetation classes are distributed in expected locations. The distribution patterns modeled by the classification appear representative of the patterns of vegetation communities at the DCP. The masked areas defined by poor texture make up close to one-eighth of the classification. These areas can largely be defined by what seems to be two flight lines of the imagery but were also identified in other portions of the imagery, specifically the south-east corner and some riparian areas.

Areal estimates (percent cover) output from OBIA for each vegetation class were calculated to evaluate the distribution of classes across the DCP (Table 4). Live PJ and

herbaceous vegetation are the dominant vegetation cover types, covering 44.06% and 22.30% of the DCP in 2014, respectively. The amount of dead piñon modeled by the OBIA for 2014 was 21.09%. This estimation of dead piñon cover is incongruous to the results of (Brewer et al. 2017) for this region where fractional estimates of dead piñon were close to 70% for the year of 2014.

Table 4. Area and over percentages for OBIA-based Vegetation Classes.

Class	Area (ha)	Percent of Total Area
Live PJ	461.37	44.06%
Dead Piñon	220.80	21.09%
Herbaceous	233.49	22.30%
Shrub	19.04	1.82%
Bare Ground	112.44	10.74%

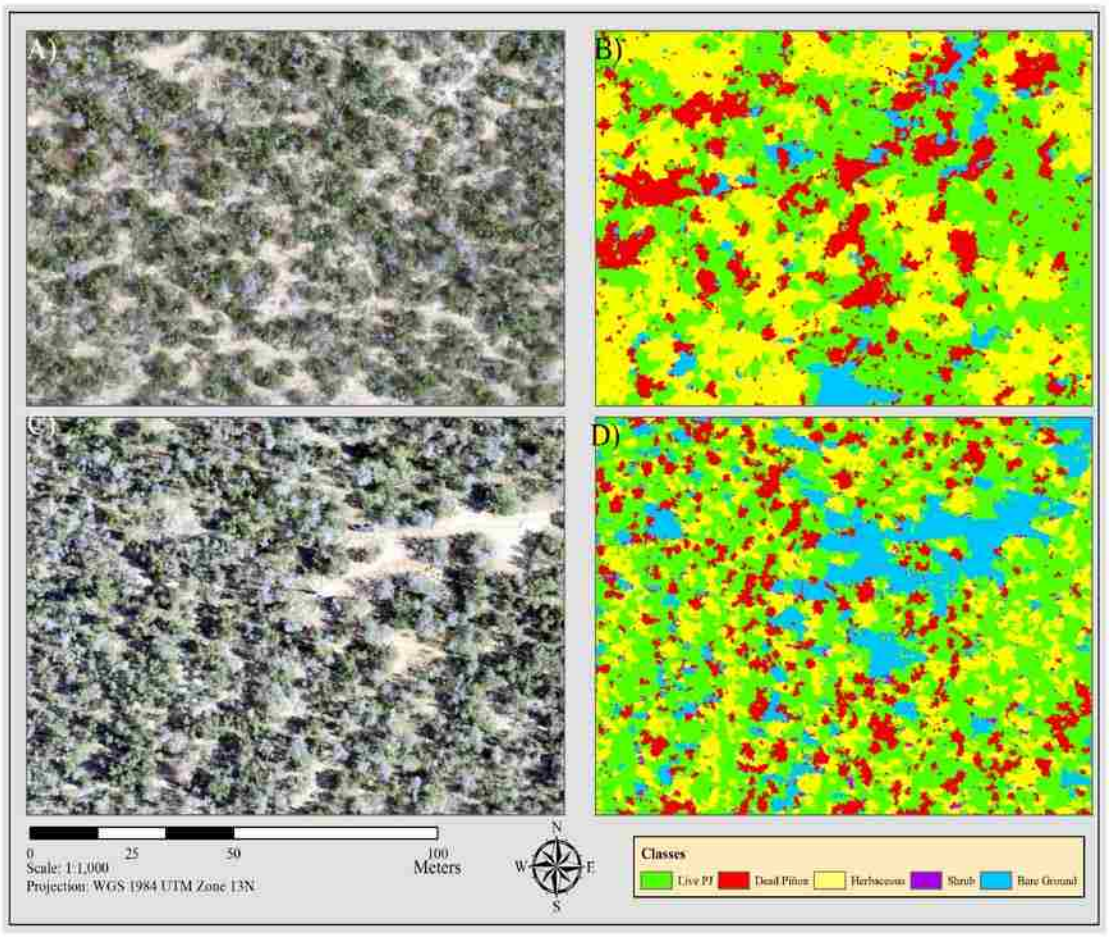

Figure 11. Deer Creek Plateau Evaluation Areas. VHR imagery and classified maps shown for the Girdled Site (A and B), and Control Site (C and D).

The PJG and PJC locations provide a visual comparison of classification results (Figure 11). At this scale, it is easier to evaluate vegetation distributions. A visual evaluation of locations near these sites indicates that at the PJC (insets C and D), both live PJ and dead piñon appear to be accurately classified in terms of location, size and shape. In contrast, at the PJG (insets A and B) both patches of live PJ and dead piñon are over classified and mixed with herbaceous/bare ground in several instances (likely due to herbaceous green-up). The PJG represents a location where there was potentially under segmentation and inaccurate classification due to low-textural contrast.

4.2 NDVI Thresholding

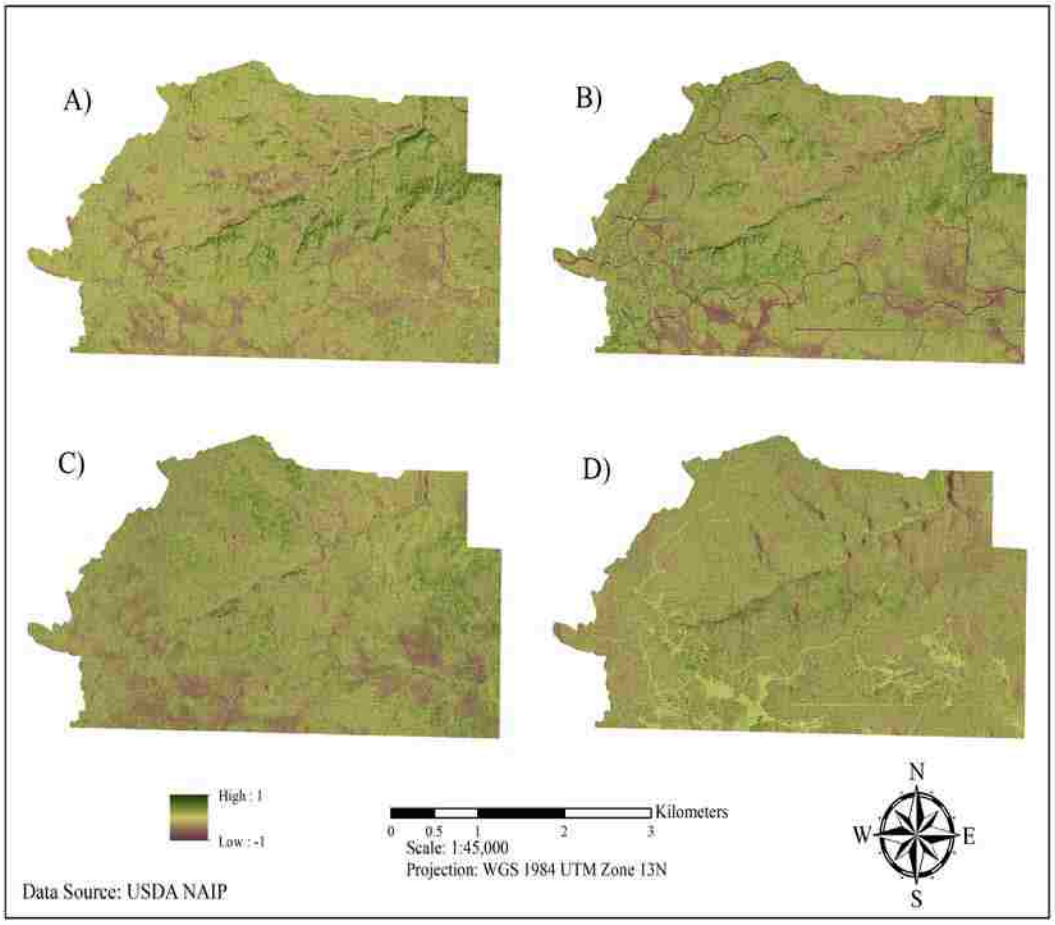

Figure 12. Normalized Difference Vegetation Index (NDVI) images for the DCP study area for: a) 2005, b) 2009, c) 2011, and d) 2014.

Evaluation of the PJG and PJC sites (Figure 13) for the NAIP image dates demonstrate that the NAIP NDVI output was sensitive to the changes observed on the ground at these sites. Insets A through C show the PJG with the 4-ha site boundary overlaid (Krofcheck et al. 2014). In 2009 (inset A) low-values of NDVI are associated with low-lying herbaceous and bare ground areas, while higher values are associated with woodland areas. For 2011 (inset B), there is a stark decrease in NDVI for these woodland

areas relating to the girdling of piñon at this site (Eitel et al. 2011). By 2014 (inset C) there is a further decrease in NDVI (resulting from mortality) among certain woodland areas due to the drought from 2011-2013 (Krofcheck et al. 2016). For the PJC, insets D through F, a similar 4-ha boundary was drawn over the site with the covariance tower located in the center. At the PJC there is little change in NDVI between 2009 (inset D) and 2011 (inset E) but there is a decrease in NDVI in low-lying herbaceous and bare ground areas. In 2014 (inset F), there is a decrease in NDVI in woodland areas.

Figure 13. NDVI images for the PJG for the years of a) 2009, b) 2011, and c) 2014, and for the PJC for the years of d) 2009, e) 2011, and f) 2014.

Changes in the distribution of live PJ to dead piñon (output from Module 2) as modeled by OBIA and derived from NAIP are documented in Figure 14. These changes

were derived from threshold values where an NDVI above 0 constituted live, and below zero constituted dead. The proportion of Live PJ to dead piñon was calculated for each image date (Figure 15). There was a small percentage of mortality that was modeled in the 2005 (7.06 ha), which increased slightly in 2009 (8.31 ha), with large increases in mortality modeled in 2011 (206.45 ha) and in 2014 (220.80 ha). While the degree of accuracy surrounding these areal estimates is unknown, the timing of these estimates largely contrast both estimates by the Litvak Lab, but also in previous studies (Krofcheck et al. 2014; Brewer et al. 2017). While mortality did occur at unprecedented rates during the drought period, these changes only occurred at the PJG in 2011, and not until 2013 for the remainder of the plateau. Therefore, while PJ may not have experienced dramatic mortality in 2011, low-lying herbaceous could have representing negative NDVI values. These values would cause confusion in the thresholding process allowing for ‘dead’ patches to be derived in locations of otherwise healthy PJ.

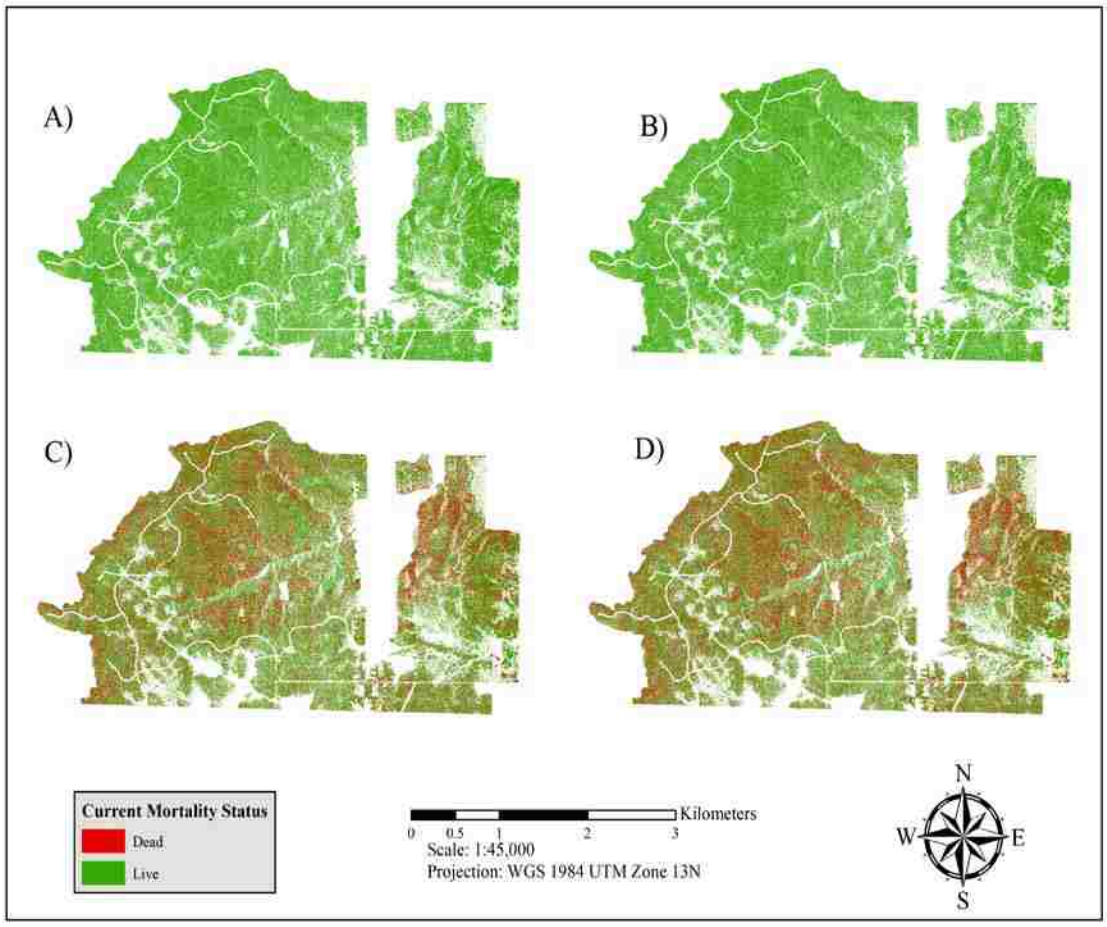

Figure 14. Map of the entire plateau showing live/dead vector boundaries for a) 2005, b) 2009, c) 2011, and d) 2014.

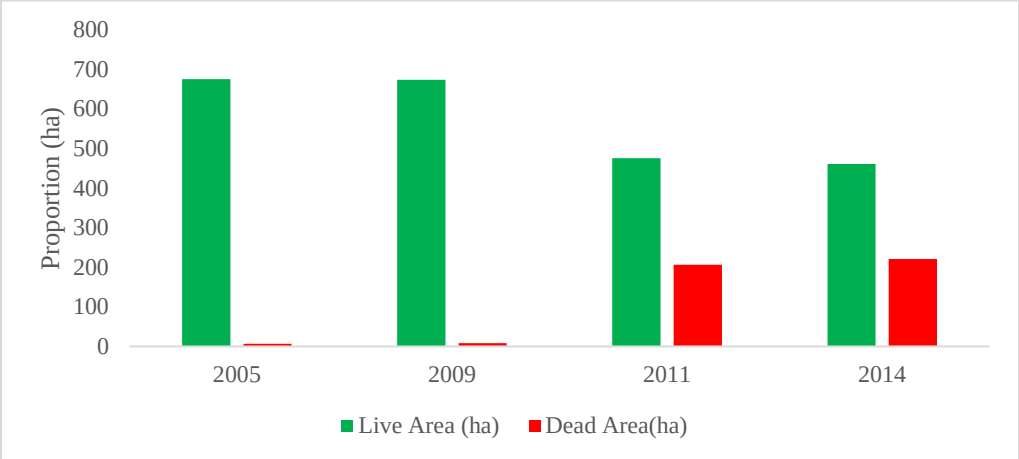

Figure 15. Proportion of live and dead PJ derived from NDVI thresholded NAIP images.

4.3 Piñon Mortality

The results from Module 3 were compiled into three sections, 1) the quantification of change over time based on NDVI thresholded NAIP images; 2) assessment of mortality patterns from Moran's I test; and 3) the evaluation of piñon-juniper mortality with respect to climate during the study period.

4.3.1 Quantification of Change

Estimates for areal coverage (for the total area of the plateau covered by PJ) as modeled by OBIA derived from NDVI thresholded NAIP images are provided in Table 4. There was a slight decrease in live PJ from 2005 (98.97% of total PJ area) to 98.82% in 2009, with a substantial decrease in live PJ to 68.64% in 2011. From 2011 to 2014 this trend continued where live PJ decreased to cover only 67.60% of the total are covered by PJ. For the entire study period as modeled by OBIA and NAIP the overall change was decrease in live PJ by 31.37% for the total area covered by live PJ.

Table 4. Estimates of Percent Change (in PJ area) from Live to Dead

Image Date	Live PJ Area (ha)	Dead Piñon Area (ha)	Mortality Increase from Previous Image Date (%)
2005	98.97%	1.03%	N/A
2009	98.82%	1.18%	14.28%
2011	68.64%	31.36%	247.5%
2014	67.60%	32.40%	6.96%

The timing and distribution of piñon mortality across the study area, and in the PJG and PJC sites is visualized in Figure 16. Similar to the outputs from Module 2, the most substantial decrease in live PJ across the entirety of the DCP as modeled by OBIA

and NAIP is 2011. More than the incongruous timing of mortality compared to previous studies, a further evaluation of the OBIA classification can be made.

Specifically, at PJC, the fine resolution boundaries for PJ still persist after being fused with the NAIP data. Similarly, the under segmented areas at the PJG also persist. Compared to the overview of increasing and decreasing NDVI values at PJG and PJC (Figure 13) an association between under segmentation and over estimation of dead piñon can be inferred. When compared to the work of the Litvak Lab, this association becomes stronger. For PJG, the OBIA classification applied to NAIP found the total PJ area to be 66.59 ha in 2009, when the Litvak in-field measurement was 29.3 for total basal area (Morillas et al. 2017). For the PJC, the OBIA measurement was 54.47 ha, when the Litvak measurement was 31.3 ha for total basal area (Morillas et al. 2017). While basal area is not a perfect metric for quantifying this difference as the imagery measurements would come from canopy measurements; it is unlikely that PJ canopies alone would represent these dramatic areal differences. Therefore, even with finer boundaries for PJG at the PJC, it is a reasonable assumption that overestimation of PJ area occurred. This overestimation would allow for low-lying herbaceous die-off and the negative NDVI values associated with it to create an over-estimation of mortality.

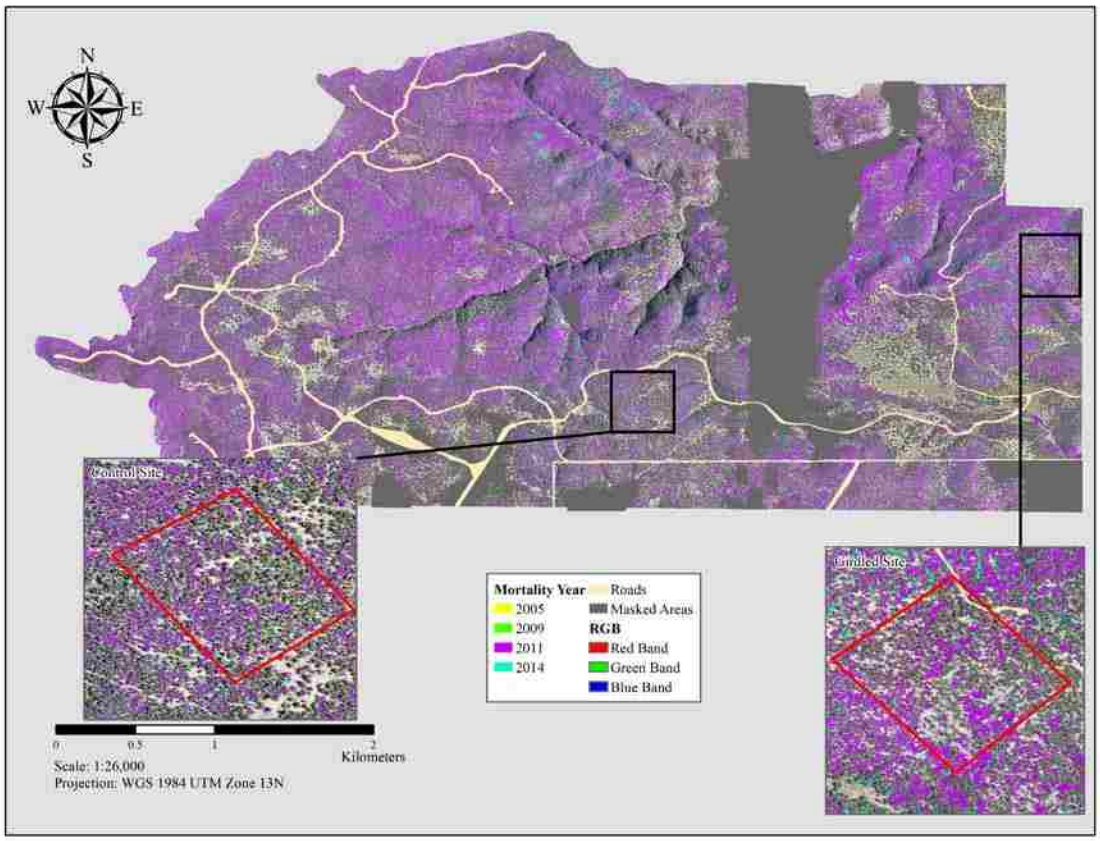

Figure 16. Map showing the location and date for mortality of PJ patches across the plateau with insets for the PJG and PJC (outlined in red).

Maps generated from image differencing the composite NDVI values (Figure 17) depict increase and decrease in PJ from one image date to the next. These maps provide a way to track the rate and distribution of change in NDVI values in PJ across the study period. Changes in NDVI for the entire study area, and within PJ segmented NDVI patches are shown in Figure 18. Both maps (Figures 17 and 18) highlight similar trends of decreasing NDVI throughout the study period with the starkest change occurring between 2009 and 2011. While this change cannot be directly attributed to mortality, it does highlight physiological stress between PJ cover and in the study region.

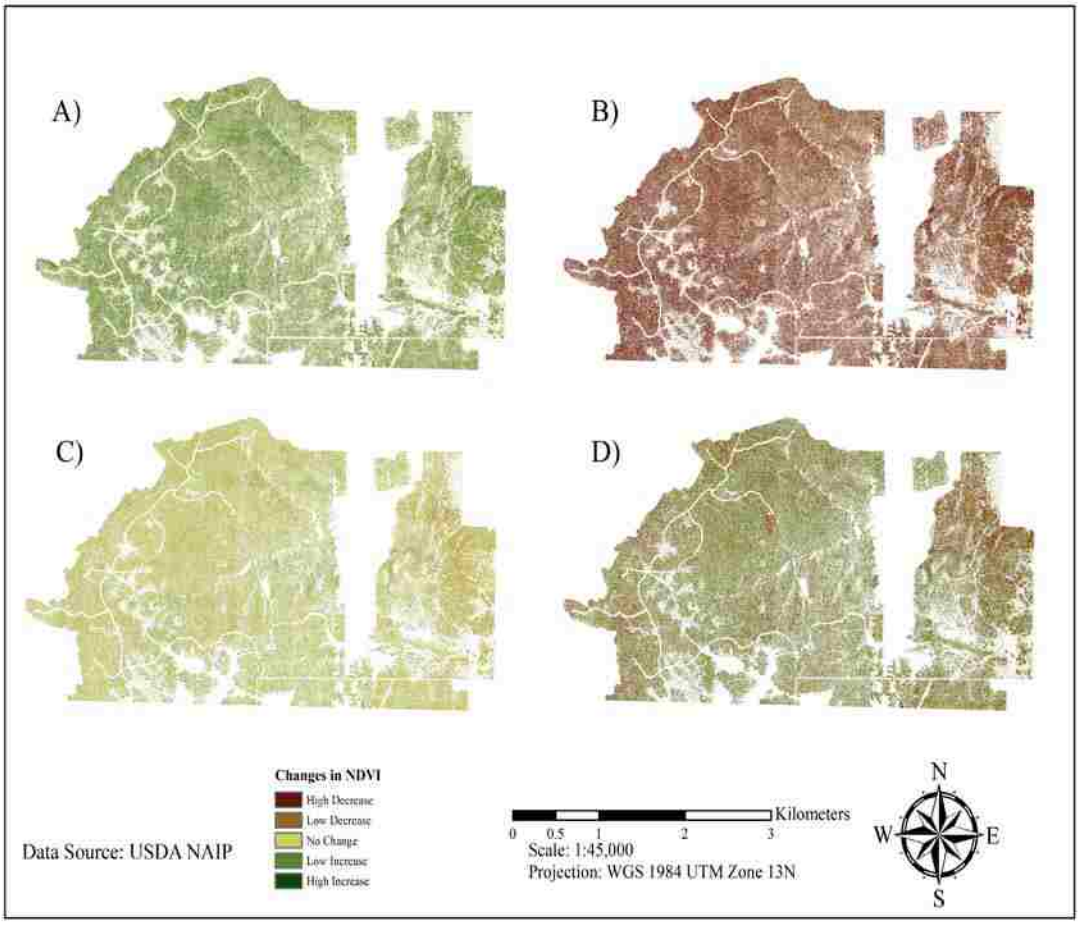

Figure 17. Map showing the results from the image differencing for a) 2005-2009, b) 2009-2011, c) 2011-2014, and d) 2005-2014.

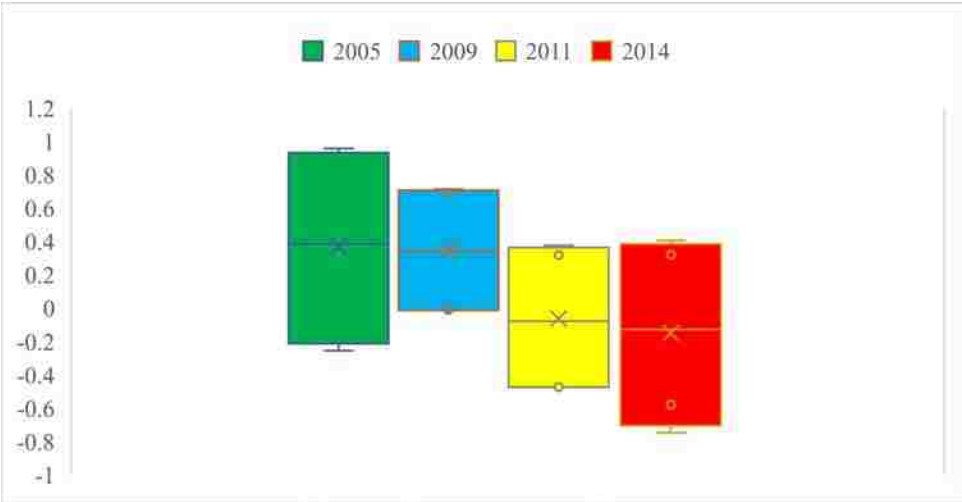

Figure 18. Box and whisker plot for values of NDVI for both the study area and patches of PJ throughout the study period

4.3.2 Spatial Patterns of Mortality

A map derived from the Moran's I test results visualizes areas of clustering of PJ mortality (Figure 19). High-high cluster areas indicate a high degree of spatial autocorrelation of negative NDVI values, which is assumed to represent dead trees. Low-Low clusters indicate the lowest degree of spatial autocorrelation of negative values; and High-Low/Low-High clusters indicate a moderate degree of spatial autocorrelation. All of these cluster distinctions present a case for spatial dependency in neighborhoods of negative NDVI values and mortality (Li, Calder, and Cressie 2007). High-High clusters have a p-value of < .01, High-Low and Low-High have a p-value between .01 and .05, and Low-Low clusters have a p-value of < .05. P-value is a measurement of probability, the values with the lowest p-values contain the highest probability of spatial autocorrelation.

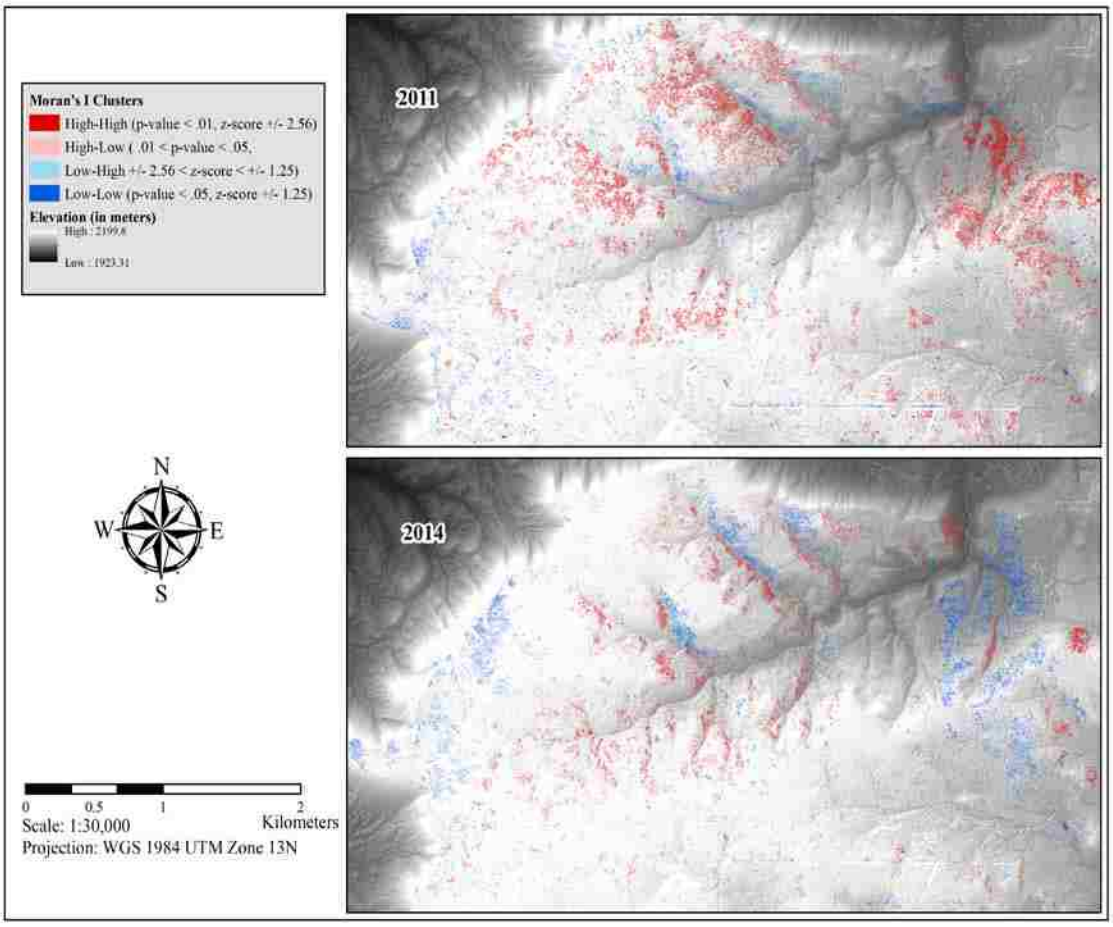

Figure 19. Map showing the locations of high (red) and low (blue) Moran's I clusters across the entire plateau. High values represent areas of high statistical significance, while low values represent areas of low statistical significance

There were no significant clusters within the dead patches for 2005 and 2009. For 2011, which would be the dead segments derived from 2009-2011, the highest degree of spatial autocorrelation among dead piñon patches occurred on the more northern portions of the study area, with some in the south-eastern portion as well. The clusters on the northern portion of the study area are located close to riparian areas of the plateau, on more northern facing aspects. In 2014, the clusters represent dead segments derived from 2011-2014, and occur in similar areas. The clusters for both 2011 and 2014 are distributed across the DCP similarly and are related by having inverse degrees of

significance, whereby locations of high clustering for 2011 were areas of low clustering for 2014.

4.3.3 Climate and Mortality Evaluation

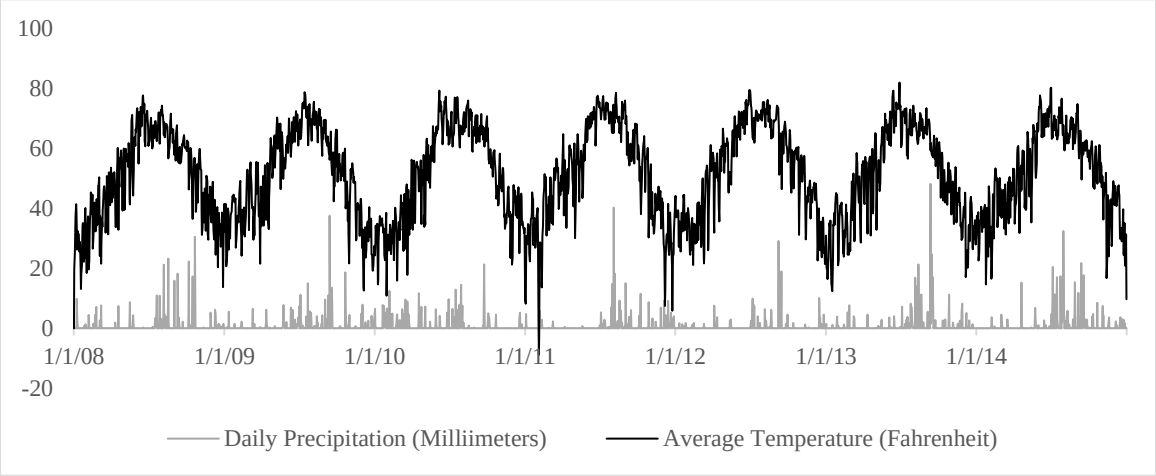

Figure 20. Climate Data for the PJG and PJC gathered by the Litvak Lab.

Precipitation and temperature data collected by the Litvak Lab at the Control and Girdled sites are shown in Figure 21. The results gathered from the NDVI thresholded maps indicated that there was an increase in NDVI for 2009 and a sharp decline in 2011. These results are gathered from NAIP data which is acquired at only one point of the year and is not representative of biomass for the entire year. For the 2009 NAIP dataset, there was 1.131 mm of average daily precipitation in the month before acquisition. In 2011, there was 0.008 mm average daily precipitation in the month before acquisition. For the entire year before the 2009 image acquisition, there was a maximum of 23 days where there was less than 1 mm of precipitation for any day in that period. Precipitation in 2011 contrasts substantially from 2009, where there was a maximum of 116 days with less than

1 mm of precipitation recorded. Both of these dry periods occur in the spring directly before the summer acquisition dates of the NAIP imagery.

Daily temperature data for 2011 depicts a climatic event that may have triggered mortality. During the first three days of February in 2011 there was a freeze that occurred. Temperatures for all three days were below 15 degrees Fahrenheit with one day being below 0. There is a possibility that temperatures this low could trigger mortality in already stressed PJ as described by Meddens et al. (2015). This mortality could be associated with the lower NDVI values recorded in the 2011 NAIP dataset. A more reasonable association that can be drawn between these NDVI values is the die-off of low-lying herbaceous cover. The minimal rainfall prior to the acquisition of the 2011 NAIP dataset would not allow for a subsequent "greening up" period by these herbaceous cover in the PJ understory (Krofcheck et al. 2016). With the lack of this herbaceous understory, there is the possibility of misclassification using NDVI due to low understory values in PJ canopies.

Chapter 5 Discussion

The results of the OBIA classification yielded two main results: a vegetation map of the DCP and estimates of piñon mortality across the DCP for previous years. While the OBIA classification did not yield high accuracies across all classes, individual accuracies for live PJ and dead piñon were high (91.43% and 84%). Accuracies for herbaceous and bare ground were relatively high (64.29% and 63.64%) with a tendency for herbaceous to be overclassified in areas where bare ground was mixed with herbaceous. The difficulty at distinguishing between low-statured vegetation types is similar to issues recorded by Laliberte et al. (2007). However, in Laliberte et al. (2007) the research goal was to yield a

high accuracy with all vegetation classes, while this study aimed to distinguish between live PJ and dead piñon (and the surrounding background) with high classification accuracy.

The shrub class was the most difficult class to accurately model. In contrast to the other classes used in this study, the shrub class was represented by multiple vegetation species. Some of the species in the shrub class were non-photosynthetic at the time of image acquisition (August, post-monsoon). Spectral heterogeneity in the shrub class resulted in confusion with the herbaceous class and the dead piñon class. Even with refinements made to the shrub class to try to improve classification accuracy, the addition of more shrub training samples did not increase accuracy. Individual shrub samples were assessed to ensure that all shrub samples were "pure" and not mixed with other classes like herbaceous or bare ground; however, leaf abscission by some shrub species during warmer drier periods make it difficult to avoid spectral confusion between shrubs and understory vegetation. Given the scale of the imagery, and the complexity of this class, it may need to be merged with the herbaceous class in future work focused on PJ mortality.

The process of creating a segmentation representative of the study area proved to be a difficult step in the OBIA procedure. The parameters used in segmentation: scale level, merge level and texture kernel size, are perhaps the most subjective portion of the OBIA process and settings are unique to each dataset. Optimal parameters for the VHR imagery used in this study were set to 35%, 85% and 5 for scale, merge, and texture kernel, respectively. The level for kernel size could be adjusted without changing the segmentation result dramatically and did not seem to affect the segmentation as much as scale and merge level. The selection of segmentation parameters is largely dependent on

the land cover patterns of the area and the target features being segmented. During preliminary trial and error efforts to derive optimal segmentation results, it was found that a higher scale level and a lower merge level could be implemented to achieve the similar segmentation results.

Between the values of scale and merge, scale largely determined the complexity of the segmentation. To appropriately segment the entire study area at a level that would allow for accurate segmentation of 'blurred' areas (instead of having to mask them out) as well as areas with lower textural variation required processing at a scale level close to 5%. Using such a low scale level generated an acceptable segmentation result, though it did not generate a satisfactory classification result. Although a high level of computational power was available for this project, the ENVI FX module would inaccurately classify and leave much of (approximately 50%) the image unclassified. This could be a residual effect of the selected scale factor, or it could be a byproduct of the size of the imagery. The PCA applied to the VHR generated a large image file size. Therefore, using a 35% scale level was the lowest computationally viable threshold that could be derived for this project. This scale level required that 'blurred' areas be masked out to avoid areas of under-segmentation and misclassification. Even after blurred areas were masked, there were still areas that seemed to be under segmented, such as the pattern shown at the PJG site. This phenomenon did not appear to persist throughout the entire study area, as shown in the segmentation in the PJC site. While scale and merge tend to play a cohesive role in segmentation, merge could largely be changed without effecting the scale factor of the segmentation. It was found that using an 85% merge level allowed for creation of segments that were representative of the target classes in regions

of high texture for the majority of the study area. Using this merge level to produce a higher accuracy classification in FX is similar to results recorded by (Meehan 2016).

To reduce under segmentation of the imagery, there is the option of creating image subsets to segment smaller areas. While this would produce smaller segments using the same parameters; it is likely that it would produce dissimilar classification outputs due to slight dissimilarities in classification inputs. In FX, the inputs for classification, example segments, are tied to specific geographic locations held within the imagery. The details for classification are derived from the segments specific to that image and cannot be extrapolated for processing on other datasets. Therefore, when performing FX on many different datasets across the same area, dissimilar results are easily produced. This problem in FX is specific to the example-based version of the module. It's hypothesized that using a rule-based classifier similar to eCognition (Trimble Navigation Limited 2012) would allow for the extrapolation of attributes across many different scenes within the same study area. While FX does have a rule-based classifier option, it would require further research to judge how well this could be implemented. As rule-based classifiers seemingly dominate the field of OBIA, there is a lot of literature surrounding the technique and how it could be implemented (Blaschke et al. 2014). Using a rule-based classified would require the user to have a seemingly explicit knowledge of the environment they are working with and how each class can be described through a certain set of rules. This process of simply defining rules can take substantial amounts of time to develop and may not even be viable during implementation. The example-based version of FX offers distinct advantages to a rule-

based classifier in certain situations; allowing the user to generate a similar product at an expedited rate by creating rules from the characteristics of selected examples.

Following initial exploration of the classifiers available in FX, the SVM classifier was selected as having the highest accuracy for classifying this dataset. Within FX there are two other options: k-means nearest neighbor or principal component analysis. The higher accuracies generated using the SVM classifier may be due to the computations SVM performs to account for posterior probabilities; these allow for a better-informed decision as to which classification attributes are most useful (Awad and Khanna 2015). This means that the user won't be penalized for the inclusion of superfluous classification attributes. Similar to the findings from this study, Meehan (2016) also reported higher classification accuracies using a support vector machine classifier in FX.

Inaccuracies in this classification could be attributed to the imagery used in this study. The imagery used in this study was flown for non-commercial education/research purposes. While this imagery was processed, it was not captured with the same requirements as many available commercial options. The imagery did contain some issues related to BDRF and are not uniform across the entire image. While the PCA transformation reduced these effects, issues related to BDRF are still persistent in some areas of the imagery. BDRF is most pronounced in the NIR band of the imagery, reducing reflectance in otherwise 'healthy' vegetation. It is unclear to what degree these issues had an effect on the vegetation classification, but are similar to issues documented by Laliberte et al. (2011). Laliberte et al. (2011) found that using aerial VHR imagery without proper radiometric calibration based on in-situ data allows for 'blurring' of

objects; whereby the radiometric values of neighbors could be interpolated to correct this phenomenon.

In addition to image inputs, the ENVI FX module allows for ancillary data layers and/or normalized-difference datasets to be included as additional input layers to segmentation and/or classification. For this research, including additional data layers did not produce satisfactory results. The inclusion of an NDVI layer in both classification and segmentation stalled the FX program and did not yield a full classification product. When the DSM was included, PJ segments were overgeneralized, likely due to the resolution differences between the VHR imagery and the DSM. Another assumption is that the DSM could only be considered as raw values instead of a canopy height model within FX. FX was not able to attribute this raw value of elevation to the specifics of any class as the study region varies in elevation by almost 200 meters, and contrasts to results reported by (Ke, Quackenbush, and Im 2010) who implemented a DSM during segmentation with success. The differences from that study are that PJ tend to grow in shorter, tight interlocking canopies, rather than as discrete individuals that would be easier to distinguish from surrounding lower-statured vegetation. Ke, Quackenbush, and Im (2010) used a smaller study site with limited terrain change where elevation could be considered a unique attribute to segment and classify target classes. An ancillary layer that could be added to this workflow to improve segmentation and classification is a canopy height model; which would allow for FX to use an object's above ground height as an attribute for segmentation and classification. Producing a canopy height model for this study area would require a digital terrain model (DTM) created either through labor intensive field work or by having Light Detection and Ranging (LiDAR) data captured

over the region. By having a DTM, it could be subtracted from the DSM to constructing a canopy height model.

OBIA applied to VHR produced maps of PJ mortality with high accuracy. Areas of PJ mortality mapped by the OBIA in conjunction with a time series of NDVI NAIP imagery proved to be a practical method for constructing a timeline of mortality. The Module 1 tool is a simple subset and NDVI calculation routine. NDVI was sensitive to changes observed on the ground at the PJG and PJC during the study period, demonstrating that this method can serve as a baseline of vegetation health for the entire study area. The products output from Modules 2 and 3 provide multiple ways to evaluate the utility of OBIA in estimating piñon mortality at the DCP. The outputs from Module 2 provided estimations of live and dead coverage but were at an earlier date and at a higher rate, likely due to under segmentation. If segments were too large there could be NDVI values from accompanying open-area herbaceous and bare ground regions causing negative NDVI values to be averaged into the composite values. Should too many of these negative values be added into the equation it would cause the composite value to read as negative and would subsequently be labeled as ‘dead.’

This assumption that under segmentation contributed to an over estimation of dead piñon in 2011 may explain the difference in mortality recorded by (Brewer et al. 2017). While the results from (Brewer et al. 2017) were generated from a subpixel analysis applied to coarser resolution data, they strongly agree with the results gathered at both the PJC and the PJG and the results of (Eitel et al. 2011; Krofcheck et al. 2014; Krofcheck et al. 2016). The long trajectory of research at the PJG and PJC sites act as useful proxies to estimate the accuracy of OBIA beyond the accuracy assessment for the

rest of the study area. These sites further provided useful proxies to judge the accuracy of the NAIP analysis. While the results of the NAIP analysis differed from the estimations gathered at those sites, to fully judge its accuracy would require either further validation sites or ecological plots.

The final output from the Module 3 tool was a spatial autocorrelation test. Performing a spatial autocorrelation test on the new segments of dead PJ for each year does offer some further insight into the utility of the OBIA approach. In areas where piñon mortality was recorded prior to drought and located in understudied regions, bark beetle activity could be an agent for mortality (Degomez and Celaya 2013). Stressed piñon are more susceptible to attack by these beetles, creating a clustering pattern of beetle attacks among neighboring piñon (Meddens et al. 2015). To test this hypothesis would require a post mortem analysis to determine where this occurred at the DCP; therefore, it serves as an inference that could be drawn from this research.

While the specifics of land cover change provided by this study cannot be taken as literal changes, a very generalized estimation of when and where piñon mortality occurred can be derived. These generalizations further provide themselves as ancillary inferences and visualizations to very thorough research objectives located at the DCP; specifically the research of (Eitel et al. 2011; Krofcheck et al. 2014; Krofcheck et al. 2016; Morillas et al. 2017).

Chapter 6 Conclusion

This study showed that OBIA applied to VHR imagery is a viable method for classification of piñon-juniper woodlands. While a total classification accuracy of higher

than 75% was not achieved, there was individual accuracies of over 90% for live PJ and over 80% dead piñon. These segments were then used to further describe and visualize mortality in Piñon-Pine across the DCP from 2005-2014. The ecological timeline of mortality provides a generalization of more complex vegetation changes, and this dataset provides a synoptic record that compliments and enhances past and future research throughout the region. This timeline and its association to the dynamic climate of the region further supports previous estimates of mortality at the Deer Creek Plateau.

Chapter 7 References

Allen, Craig D., Alison K. Macalady, Haroun Chenchouni, Dominique Bachelet, Nate McDowell, Michel Vennetier, Thomas Kitzberger, et al. 2010. "A Global Overview of Drought and Heat-Induced Tree Mortality Reveals Emerging Climate Change Risks for Forests." *Forest Ecology and Management* 259 (4): 660–684. doi:10.1016/j.foreco.2009.09.001.

Awad, Mariette, and Rahul Khanna. 2015. "Support Vector Machines for Classification." In *Efficient Learning Machines*, 39–66. doi:10.1007/978-1-4302-5990-9_3.

Blaschke, Thomas. 2010. "Object Based Image Analysis for Remote Sensing." *ISPRS Journal of Photogrammetry and Remote Sensing* 65 (1). Elsevier B.V.: 2–16. doi:10.1016/j.isprsjprs.2009.06.004.

Blaschke, Thomas, Geoffrey J. Hay, Maggi Kelly, Stefan Lang, Peter Hofmann, Elisabeth Addink, Raul Queiroz Feitosa, et al. 2014. "Geographic Object-Based Image Analysis - Towards a New Paradigm." *ISPRS Journal of Photogrammetry and Remote Sensing* 87. International Society for Photogrammetry and Remote Sensing, Inc. (ISPRS): 180–191. doi:10.1016/j.isprsjprs.2013.09.014.

Breshears, David D., Orrin B. Myers, Clifton W. Meyer, Fairley J. Barnes, Chris B. Zou, Craig D. Allen, Nathan G. McDowell, and William T. Pockman. 2009. "Research Communications Research Communications Tree Die-off in Response to Global Change-Type Drought: Mortality Insights from a Decade of Plant Water Potential Measurements." *Frontiers in Ecology and the Environment* 7 (4): 185–189. doi:10.1890/080016.

Brewer, William, Caitlin L. Lippitt, Christopher D. Lippitt, and Marcy E. Litvak. 2017. "Assessing Drought-Induced Change in a Piñon-Juniper Woodland with Landsat: A Multiple Endmember Spectral Mixture Analysis Approach." *International Journal of Remote Sensing* 38 (14). Taylor & Francis: 4156–4176. doi:10.1080/01431161.2017.1317940.

Clifford, Michael J., Neil S. Cobb, and Michaela Buenemann. 2011. "Long-Term Tree Cover Dynamics in a Pinyon-Juniper Woodland: Climate-Change-Type Drought Resets Successional Clock." *Ecosystems* 14 (6): 949–962. doi:10.1007/s10021-011-9458-2.

Colomina, I., and P. Molina. 2014. "Unmanned Aerial Systems for Photogrammetry and Remote Sensing: A Review." *ISPRS Journal of Photogrammetry and Remote Sensing* 92. International Society for Photogrammetry and Remote Sensing, Inc. (ISPRS): 79–97. doi:10.1016/j.isprsjprs.2014.02.013.

Davies, Kirk W., Steven L. Petersen, Dustin D. Johnson, D. Bracken Davis, Matthew D. Madsen, Daniel L. Zvirzdin, and Jon D. Bates. 2010. "Estimating Juniper Cover From National Agriculture Imagery Program (NAIP) Imagery and Evaluating Relationships Between Potential Cover and Environmental Variables." *Rangeland Ecology & Management* 63 (6): 630–637. doi:10.2111/REM-D-09-00129.1.

Degomez, Tom, and Bob Celaya. 2013. *The Piñon Ips Bark Beetle*.

Eitel, Jan U H, Lee A. Vierling, Marcy E. Litvak, Dan S. Long, Urs Schulthess, Alan A. Ager, Dan J. Krofcheck, and Leo Stoscheck. 2011. "Broadband, Red-Edge Information from Satellites Improves Early Stress Detection in a New Mexico Conifer Woodland." *Remote Sensing of Environment* 115 (12): 3640–3646. doi:10.1016/j.rse.2011.09.002.

Evans, Raymond A, and USDA Forest Serivce. 1988. *Management of Pinyon-Juniper Woodlands*.

Gandhi, G. Meera, S. Parthiban, Nagaraj Thummalu, and A. Christy. 2015. "NDVI: Vegetation Change Detection Using Remote Sensing and GIS - A Case Study of Vellore District." *Procedia Computer Science* 57. Elsevier Masson SAS: 1199–1210. doi:10.1016/j.procs.2015.07.415.

Gaylord, Monica L, Thomas E Kolb, William T Pockman, Jennifer a Plaut, Enrico a Yepez, Alison K Macalady, Robert E Pangle, and Nate G Mcdowell. 2013. "Drought Predisposes Pinon– Juniper Woodlands to Insect Attacks Drought Predisposes Piñon–Juniper Woodlands to Insect Attacks and Mortality." *New Phytologist*, 567–578. doi:10.1111/nph.12174.

Harris Geospatial. 2008. "ENVI Feature Extraction Module User's Guide."

Hayes, Matthew M., Scott N. Miller, and Melanie A. Murphy. 2014. "High-Resolution Landcover Classification Using Random Forest." *Remote Sensing Letters* 5 (2). Taylor & Francis: 112–121. doi:10.1080/2150704X.2014.882526.

Hulet, April, Bruce A. Roundy, Steven L. Petersen, Stephen C. Bunting, Ryan R. Jensen, and Darrell B. Roundy. 2014. "Utilizing National Agriculture Imagery Program Data to Estimate Tree Cover and Biomass of Piñon and Juniper Woodlands." *Rangeland Ecology & Management* 67 (5): 563–572. doi:10.2111/REM-D-13-00044.1.

IPCC. 2014. "Part A: Global and Sectoral Aspects. (Contribution of Working Group II to the Fifth Assessment Report of the Intergovernmental Panel on Climate Change)." *Climate Change 2014: Impacts, Adaptation, and Vulnerability.*, 1132. https://www.ipcc.ch/pdf/assessment-report/ar5/wg2/WGIIAR5-FrontMatterA_FINAL.pdf.

Jensen, John R. 2005. *Introductory Digital Image Processing*. 3rd ed. Pearson Prentice Hall.

Kamal, Muhammad, Stuart Phinn, and Kasper Johansen. 2015. *Object-Based Approach for Multi-Scale Mangrove Composition Mapping Using Multi-Resolution Image Datasets*. *Remote Sensing*. Vol. 7. doi:10.3390/rs70404753.

Ke, Yinghai, Lindi J. Quackenbush, and Jungho Im. 2010. "Synergistic Use of QuickBird Multispectral Imagery and LIDAR Data for Object-Based Forest Species Classification." *Remote Sensing of Environment* 114 (6). Elsevier Inc.: 1141–1154. doi:10.1016/j.rse.2010.01.002.

Knipling, Edward B. 1970. “Physical and Physiological Basis for the Reflectance of Visible and Near-Infrared Radiation from Vegetation.” *Remote Sensing of Environment*, no. 1: 155–159.

Knoth, Christian, Birte Klein, Torsten Prinz, and Till Kleinebecker. 2013. “Unmanned Aerial Vehicles as Innovative Remote Sensing Platforms for High-Resolution Infrared Imagery to Support Restoration Monitoring in Cut-over Bogs.” *Applied Vegetation Science* 16 (3): 509–517. doi:10.1111/avsc.12024.

Krofcheck, Dan J., Jan U.H. Eitel, Christopher D. Lippitt, Lee A. Vierling, Urs Schulthess, and Marcy E. Litvak. 2016. “Remote Sensing Based Simple Models of GPP in Both Disturbed and Undisturbed Piñon-Juniper Woodlands in the Southwestern U.S.” *Remote Sensing* 8 (1). doi:10.3390/rs8010020.

Krofcheck, Dan J., Jan U.H. Eitel, Lee A. Vierling, Urs Schulthess, Timothy M. Hilton, Eva Dettweiler-Robinson, Rosemary Pendleton, and Marcy E. Litvak. 2014. “Detecting Mortality Induced Structural and Functional Changes in a Piñon-Juniper Woodland Using Landsat and RapidEye Time Series.” *Remote Sensing of Environment* 151. Elsevier Inc.: 102–113. doi:10.1016/j.rse.2013.11.009.

Krofcheck, Dan J, and Marcy Litvak. 2014. “Bridging Structure and Function in Semi-Arid Ecosystems by Integrating Remote Sensing and Ground Based Measurements.”

Laliberte, Andrea S., Mark A. Goforth, Caitriana M. Steele, and Albert Rango. 2011. “Multispectral Remote Sensing from Unmanned Aircraft: Image Processing Workflows and Applications for Rangeland Environments.” *Remote Sensing* 3 (11): 2529–2551. doi:10.3390/rs3112529.

Laliberte, Andrea S., Albert Rango, Jeffrey Herrick, Ed Fredrickson, and Laura Burkett. 2007. “An Object-Based Image Analysis Approach for Determining Fractional Cover of Senescent and Green Vegetation with Digital Plot Photography.” *Journal of Arid Environments* 69 (1): 1–14. doi:10.1016/j.jaridenv.2006.08.016.

Lehmann, Jan Rudolf Karl, Felix Nieberding, Torsten Prinz, and Christian Knoth. 2015. “Analysis of Unmanned Aerial System-Based CIR Images in Forestry-a New Perspective to Monitor Pest Infestation Levels.” *Forests* 6 (3): 594–612. doi:10.3390/f6030594.

Li, Hongfei, Catherine A. Calder, and Noel Cressie. 2007. “Beyond Moran’s I: Testing for Spatial Dependence Based on the Spatial Autoregressive Model.” *Geographical Analysis* 39 (4): 357–375. doi:10.1111/j.1538-4632.2007.00708.x.

Lippitt, Christopher D. 2015. “Perspectives From The Field: Remote Sensing from Small Unmanned Platforms: A Paradigm Shift.” *Environmental Practice* 17 (03): 235–236. doi:10.1017/S1466046615000204.

Liu, Desheng, Maggi Kelly, Peng Gong, and Qinghua Guo. 2007. “Characterizing Spatial-Temporal Tree Mortality Patterns Associated with a New Forest Disease.” *Forest Ecology and Management* 253 (1–3): 220–231. doi:10.1016/j.foreco.2007.07.020.

Maxwell, Susan K. 2011. “Generating Land Cover Boundaries from Remotely Sensed Data Using Object-Based Image Analysis: Overview and Epidemiological Application.” *Spat Spatiotemporal Epidemiol* 1 (4): 231–237. doi:10.1016/j.sste.2010.09.005.Generating.

Meddens, Arjan J H, Jeffrey A. Hicke, Alison K. Macalady, Polly C. Buotte, Travis R. Cowles, and Craig D. Allen. 2015. “Patterns and Causes of Observed Piñon Pine Mortality in the Southwestern United States.” *New Phytologist* 206 (1): 91–97. doi:10.1111/nph.13193.

Meehan, Kelly. 2016. “Object Based Image Analysis Technique for Distinguishing Tropical Native Forest from Plantations: A Landcover Classification Analysis of Patches Surrounding the Serra Do Brigadeiro State Park, Minas Gerais, Brazil.” Duke University.

Moran, P. A. P. 1950. “Notes on Continuous Stochastic Phenomena.” *Biometrika* 37 (1): 17–23.

Morillas, L., R. E. Pangle, G. E. Maurer, W. T. Pockman, N. McDowell, C. W. Huang, D. J. Krofcheck, et al. 2017. “Tree Mortality Decreases Water Availability and Ecosystem Resilience to Drought in Piñon-Juniper Woodlands in the Southwestern U.S.” *Journal of Geophysical Research: Biogeosciences* 122 (12): 3343–3361. doi:10.1002/2017JG004095.

Moskal, L. Monika, Diane M. Styers, and Meghan Halabisky. 2011. “Monitoring Urban Tree Cover Using Object-Based Image Analysis and Public Domain Remotely Sensed Data.” *Remote Sensing* 3 (10): 2243–2262. doi:10.3390/rs3102243.

Mueller, Rebecca C., Crescent M. Scudder, Marianne E. Porter, R. Talbot Trotter, Catherine A. Gehring, and Thomas G. Whitham. 2005. “Differential Tree Mortality in Response to Severe Drought: Evidence for Long-Term Vegetation Shifts.” *Journal of Ecology* 93 (6): 1085–1093. doi:10.1111/j.1365-2745.2005.01042.x.

National Park Service. 2017. “Pinyon-Juniper Woodlands - Introduction & Distribution.” https://www.nps.gov/articles/pinyon-juniper-woodlands-distribution.htm.

OPUS National Geodetic Survey. “Online Positioning User Service.”

Ortiz, Sonia M., Johannes Breidenbach, and Gerald Kändler. 2013. “Early Detection of Bark Beetle Green Attack Using TerraSAR-X and Rapideye Data.” *Remote Sensing* 5 (4): 1912–1931. doi:10.3390/rs5041912.

PRISM Climate Group, Oregon State University. “PRISM Climate Data.”

Roberts, D A, M O Smith, and J B Adams. 1993. “Green,Vegetation, Nonphotosynthetic Vegetation, and Soil in AVIRIS Data.” *Remote Sensing of Environment* V. 44 (N. 2/3): 255–269.

Rouse, J.W., R.H. Haas, J.A. Schiel, and D.A. Deering. 1973. “Monitoring Vegetation Systems in the Great Plains with ERTS.” In *Proceedings of Third Earth Resources Technology Satellite - 1 Symposium*, 3010–3017.

Ryherd, Soren, and Curtis Woodcock. 1996. “Combining Spectral and Texture Data in the Segmentation of Remotely Sensed Images.” *Photogrammetric Engineering Remote Sensing* 62 (2): 181–194. http://www.asprs.org/publications/pers/96journal/february/1996_feb_181-194.pdf.

Shaw, John D, Brytten E Steed, and Larry T DeBlander. 2005. “Forest Inventory and Analysis (FIA) Annual Inventory Answers the Question: What Is Happening to Pinyon-Juniper Woodlands?” *Journal of Forestry* 103: 280–285.

Sonwalkar, Mukul, Li Fang, and Donglian Sun. 2010. “Use of NDVI Dataset for a GIS Based Analysis: A Sample Study of TAR Creek Superfund Site.” *Ecological Informatics* 5 (6). Elsevier B.V.: 484–491. doi:10.1016/j.ecoinf.2010.07.003.

South Central Climate Science Center. 2013. *Drought History for the Central Highlands of New Mexico*.

Stoyan, Dietrich, and Antti Penttinen. 2000. “Recent Applications of Point Process Methods in Forestry Statistics.” *Statistical Science* 15 (1): 61–78. doi:10.1126/science.1193771.

Strahler, Alan H., Curtis E. Woodcock, and James A. Smith. 1986. “On the Nature of Models in Remote Sensing.” *Remote Sensing of Environment* 20 (2): 121–139. doi:10.1016/0034-4257(86)90018-0.

Trimble Navigation Limited. 2012. “ECognition User Guide 9,” no. August: 1–5.

USDA Farm Service Agency. 2006. *FSA’s GIS Activities at the Aerial Photography Field Office (APFO)*. https://www.fsa.usda.gov/programs-and-services/aerial-photography/imagery-programs/naip-imagery/.

Williams, Park, Craig D Allen, Alison K Macalady, Daniel Griffin, Connie A Woodhouse, David M Meko, Thomas W Swetnam, et al. 2012. “Temperature as a Potent Driver of Regional Forest Drought Stress and Tree Mortality.” *Nature Climate Change* 3 (3). Nature Publishing Group: 292–297. doi:10.1038/nclimate1693.

Williams, Park, Craig D Allen, Constance I Millar, Thomas W Swetnam, Joel Michaelsen, Christopher J Still, and Steven W Leavitt. 2010. “Forest Responses to Increasing Aridity and Warmth in the Southwestern United States.” *Proceedings of the National Academy of Sciences of the United States of America* 107 (50): 21289–21294. doi:10.1073/pnas.0914211107.